Cell Reports

Article

Non-gonadal PIWIL1/Aubergine drives regenerative and tumorigenic stem cell proliferation in the intestine

Graphical abstract

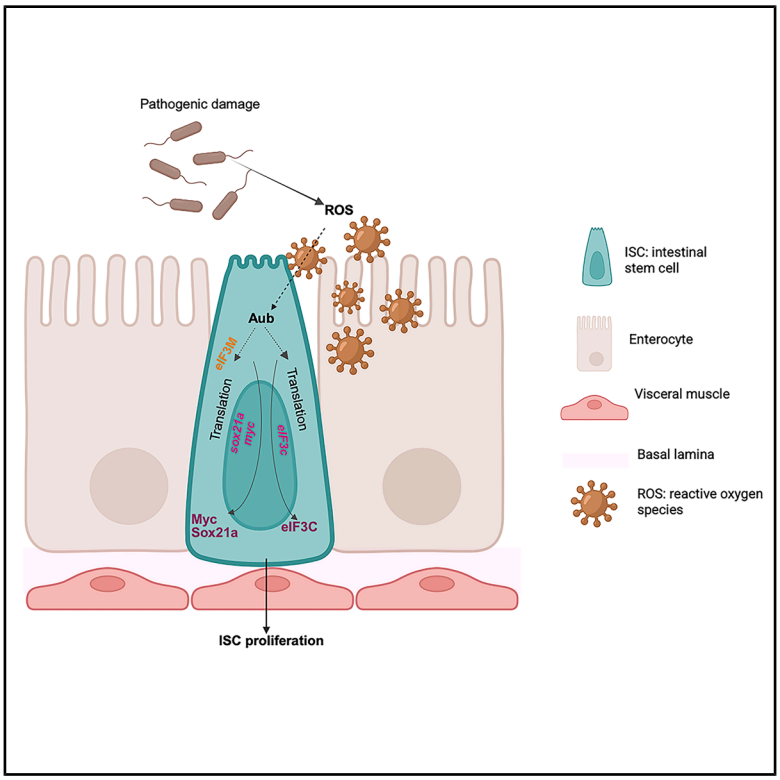

Highlights

- Oxidative stress upregulates Aubergine (Aub) in *Drosophila* intestinal stem cells (ISCs)
- Aub and PIWIL1 drive tumorigenesis in the *Drosophila* and human intestine, respectively
- Aub drives protein synthesis in regenerating ISC, including Sox21a and Myc
- Roles of Aub in regenerating ISCs involve eIF3M and eIF3C and are piRNA independent

Authors

Karen Bellec, Lynsey R. Carroll, Kathryn A.F. Pennel, ..., Kevin Myant, Rippei Hayashi, Julia B. Cordero

Correspondence

rippei.hayashi@anu.edu.au (R.H.), julia.cordero@glasgow.ac.uk (J.B.C.)

In brief

Expression and function of classical germline genes are reported in somatic tissues. Bellec et al. report damage-inducible upregulation and function of the PIWI protein Aubergine in regenerating intestinal stem cells. Roles of Aubergine in the adult intestine involve translation of essential stem cell factors and are uncoupled from piRNA regulation.

Bellec et al., 2026, Cell Reports *45*, 117186
April 28, 2026
https://doi.org/10.1016/j.celrep.2026.117186

CellPress

Cell Reports

CellPress
OPEN ACCESS

Article

Non-gonadal PIWIL1/Aubergine drives regenerative and tumorigenic stem cell proliferation in the intestine

Karen Bellec,[1] Lynsey R. Carroll,[1] Kathryn A.F. Pennel,[1] Yuanliangzi Tian,[1] Yachuan Yu,[2] Aslihan Bastem Akan,[3,4,7] Caroline V. Billard,[3,4] Nora Doleschall,[3,4] Alexander R. Cameron,[1] Fabiana Herédia,[5,6] Alisson M. Gontijo,[5,6] Anna M. Ochocka-Fox,[4,7] James P. Blackmur,[4,7] Farhat V.N. Din,[4,7] Malcolm G. Dunlop,[4,7] Joanne Edwards,[1] Kevin Myant,[3,4] Rippei Hayashi,[8,9,*] and Julia B. Cordero[1,2,10,*]

[1]Wolfson Wohl Cancer Research Centre, School of Cancer Sciences, University of Glasgow, Garscube Estate, Switchback Road, Glasgow G61 1QH, UK
[2]CRUK Scotland Institute, Garscube Estate, Switchback Road, Glasgow G61 1BD, UK
[3]Colorectal Stem Cell Transformation Group, Institute of Genetics and Cancer, The University of Edinburgh, Western General Hospital Campus, Crewe Road, Edinburgh EH4 2XU, UK
[4]Cancer Research UK Scotland Centre, Institute of Genetics and Cancer, The University of Edinburgh, Western General Hospital, Crewe Road South, Edinburgh, EH4 2XR, UK
[5]iNOVA4Health, Nova Medical School, Faculdade de Ciências Médicas, NMS, FCM, Nova University of Lisbon, Lisbon, Portugal
[6]cE3c - Centre for Ecology, Evolution and Environmental Changes & CHANGE - Global Change and Sustainability Institute, Department of Animal Biology, Faculty of Sciences, University of Lisbon, Lisbon, Portugal
[7]Colon Cancer Genetics Group, Institute of Genetics and Cancer, The University of Edinburgh, Western General Hospital Campus, Crewe Road, Edinburgh EH4 2XU, UK
[8]John Curtin School of Medical Research, The Australian National University, Acton, ACT, Australia
[9]The Shine-Dalgarno Centre for RNA Innovation, The Australian National University, Acton, ACT, Australia
[10]Lead contact
*Correspondence: rippei.hayashi@anu.edu.au (R.H.), julia.cordero@glasgow.ac.uk (J.B.C.)
https://doi.org/10.1016/j.celrep.2026.117186

SUMMARY

The PIWI-interacting RNA (piRNA) biosynthesis pathway is best studied for its role in suppressing *Drosophila* germline transposable elements. Piwi, the founding member of the pathway, is involved in adult intestinal stem cell (ISC) homeostasis. Whether a broader role of the PIWI pathway exists in the intestine remains unknown. Here, we characterize a role of the PIWI family protein Aubergine (Aub) in ISCs. While dispensable for basal ISC self-renewal, upregulation of Aub by damage-induced reactive oxygen species drives regenerative ISC proliferation through increased protein synthesis, including translation of ISC factors Myc and Sox21a. Unexpectedly, such roles of Aub in ISCs appear uncoupled from its piRNA regulatory function. Additionally, Aub and mammalian PIWIL1 mediate tumorigenic intestinal growth in *Drosophila* and human organoids, respectively. Our results reveal regulated protein translation as a fundamental aspect of regenerative ISC function and discover a central role of Aub in such process.

INTRODUCTION

Since their discovery in *Drosophila melanogaster*,[1–3] the PIWI protein family has been extensively studied for their conserved role protecting germline genome integrity via piRNA-dependent transposable element (TE) silencing.[4–13] piRNAs are PIWI protein-bound 24–32 nucleotides long small non-coding RNAs derived from transposon-dense genomic loci called piRNA clusters.[6] PIWI proteins loaded with a piRNA exert gene silencing by cleaving mRNAs or recruiting chromatin modification enzymes to install heterochromatin. In the *Drosophila* germline, PIWI proteins Piwi and Aubergine (Aub) mainly bind piRNAs that target TEs in the nucleus and the cytoplasm, respectively,[6,14–16] while Argonaute 3 (AGO3) predominantly binds TE sense piRNAs to aid the production of TE antisense piRNAs through the ping-pong pathway.[6,7,17–20]

Numerous reports have documented the presence of PIWI proteins in somatic tissues and/or roles for these proteins beyond piRNAs and TE regulation,[21–31] including roles of Piwi in the maintenance of adult *Drosophila* intestinal stem cells.[27,28] However, it remains unclear whether there is a general role of the PIWI pathway and piRNAs in the adult intestine or if PIWI proteins play roles distinct from their canonical piRNA-dependent function.

Here, we discovered that Aub is upregulated within the stem/progenitor compartment of the adult midgut in response to oxidative stress and is required to regulate regenerative and hyperplastic ISC proliferation. Despite the presence of piRNA-like

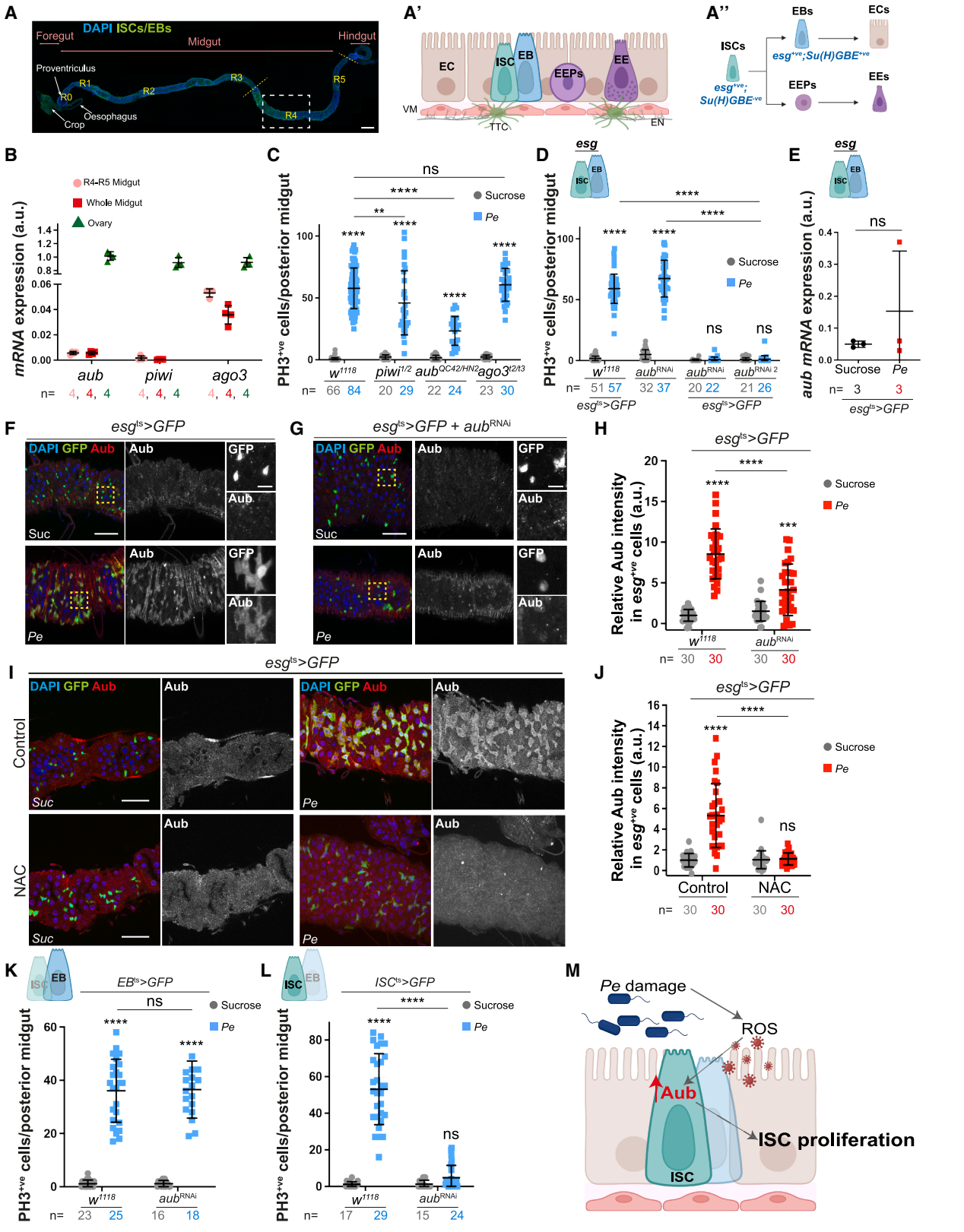

(legend on next page)

molecules in ISCs/EBs, our studies indicate that the induction of ISC proliferation by Aub is uncoupled from its canonical piRNA regulatory function. Mechanistically, Aub promotes protein synthesis in regenerating ISCs, including translation of stem cell factors Myc and Sox21a. Furthermore, Aub or its mammalian orthologue PIWIL1 drives tumorigenic intestinal growth in the midgut and human intestinal organoids, respectively. Altogether, our results uncover non-canonical roles of Aub and PIWIL1 in physiological and pathological proliferation of the adult intestine *in vivo*.

RESULTS

Aub is required for regenerative proliferation of ISCs following damage to the adult midgut epithelium

The adult *Drosophila* midgut epithelium is maintained and repaired by intestinal stem cells (ISCs).[32,33] Undifferentiated stem cell progeny, namely, enteroblasts (EBs; Figure 1A, A′) and pre-enteroendocrine cells are precursors of absorptive enterocytes (ECs) and secretory enteroendocrine cells (EEs; Figure 1A',A″), respectively.[34–36] Visceral muscle (VM), terminal tracheal cells (TTCs), and enteric neurons (ENs; Figure 1A') compose the intestinal microenvironment.[37,38]

RT-qPCR analysis of midguts from mated females showed low but detectable levels of *piwi*, *aub* and *ago3* mRNAs in homeostatic midguts, including the posterior midgut (R4–R5; Figures 1A and 1B).[39,40] We next assessed the role of the PIWI pathway in intestinal regeneration upon oral infection with the pathogen *Pseudomonas entomophila* (*Pe*)[41] and quantified proliferating ISCs by phosphorylated histone H3 (PH3) staining (Figures 1C and S1A). *Pe* feeding caused robust ISC proliferation in wild type (w^{1118}) flies when compared to their sucrose fed counterparts (Figures 1C and S1A). While loss of *piwi* mildly diminished intestinal regeneration (Figures 1C and S1A), aub^{HN2}/aub^{QC42} loss of function mutants[19,20,42,43] depicted strong impairment in midgut regeneration (Figures 1C and S1A). Knockdown of *aub* within ISCs and EBs (stem/progenitors) by RNAi overexpression under the control of the temperature-sensitive *escargot-Gal4* (esg^{ts}) abolished regenerative ISC proliferation (Figures 1D and S1B). On the other hand, ISC lineage tracing by mosaic analysis with a repressible cell marker (MARCM),[44] revealed that, unlike *piwi,*[28] knocking down *aub* did not cause any detectable effects in homeostatic ISC self-renewal (Figures S1C and S1D). Unexpectedly, loss of *ago3*, an obligate partner of *aub* in the ping-pong pathway, had no impact on intestinal regeneration upon damage (Figures 1C and S1A). Similarly, we detected no effect on intestinal regeneration upon loss of *spnE* (Figure S1E), an essential ping-pong pathway RNA helicase.[20,45] These data point to a distinctive role of *aub* in regenerative ISC proliferation of the adult *Drosophila* midgut.

Damage-induced oxidative stress drives post-transcriptional upregulation of Aub in regenerating stem/progenitor cells of the adult *Drosophila* midgut

RT-qPCR experiments in sorted ISCs/EBs, identified by their enrichment of *esg* mRNA expression (Figure S1F), revealed overall enrichment of *aub* in sorted cells versus whole midgut values (Figures 1B and 1E), but they did not show significant changes in *aub* mRNA upon *Pe* infection (Figure 1E). On the other hand, protein immunostaining experiments revealed strong upregulation of Aub expression in ISCs/EBs upon midgut damage (Figure 1F, H), which was markedly reduced following *esg-Gal4*-driven RNAi *aub* knockdown (Figures 1G and 1H).

Intestinal damage triggered by pathogenic bacterial infection generates high levels of reactive oxygen species (ROS) in the gut lumen, mainly via enterocytes (ECs), as a protective host mechanism against the pathogen.[46] ROS also play an important role as signaling molecules influencing the production, secretion, and stability of intestinal and niche-derived factors necessary to induce ISC proliferation during midgut regeneration.[47,48] Consistently, blocking ROS in *Pe*-infected midguts by feeding animals with the antioxidant *N-acetyl cysteine* (NAC) led to significant impairment of Aub upregulation upon damage (Figures 1I and 1J). However, blocking ISC proliferation in the presence of infection did not impact Aub upregulation (Figures S1G–S1J). These results suggest that pathogenic damage-induced upregulation of Aub is dependent on oxidative stress and precedes the activation of regenerative ISC proliferation.

Aub works cell autonomously in ISCs to drive midgut regeneration upon damage

Similarly to mammalian Paneth cells, EBs are components of the *Drosophila* intestinal stem cell niche.[49,50] Wg/Wnt secretion from EBs is essential to paracrinally induce regenerative ISC

Figure 1. ISC Aub drives regenerative proliferation in the *Drosophila* midgut

(A) Mated female gut. ISCs and EBs (GFP; green). DAPI (blue) stains all nuclei. Yellow lines delineate posterior midgut, and the rectangle defines the region of interest throughout the study. Scale bar, 200 μm. (A′ and A″) Schematics of midgut epithelium and associated tissues (A′); ISC lineage (A″). ISCs, intestinal stem cells; EBs, enteroblasts; EEPs, enteroendocrine cell precursors; ECs, enterocytes; EEs, enteroendocrine cells; VM, visceral muscle; EN, enteric neurons; and TTC, terminal tracheal cell.

(B) *aub*, *piwi*, and *ago3* expression in midgut and ovary. n = biological replicates.

(C) PH3 cells in midguts from w^{1118}, *aub*, *piwi*, or *ago3* mutant flies.

(D) PH3 cells in control midguts (esg^{ts}>*GFP* or UAS-aub^{RNAi} only) or overexpressing independent *aub-RNAis* within ISCs/EBs (esg^{ts}>*GFP* + aub^{RNAi} or aub^{RNAi2}).

(E) *aub* expression in sorted ISCs/EBs. Mann-Whitney *t* test. n = biological replicates.

(F and G) Aub staining (red and gray) in control or aub^{RNAi} midguts. Yellow squares delineate the magnified area in righthand panels.

(H) Quantification of data in (F) and (G). n = number of cells.

(I) Aub staining (red; gray) in midguts upon sucrose or *Pe* feeding, with or without the antioxidant *N-acetyl cysteine* (NAC).

(J) Quantification of data in (I). n = number of cells.

(K and L) PH3 cells in midguts overexpressing aub^{RNAi} in either EBs (K) or ISCs (L).

(M) Schematic of Aub regulation and function in regenerating ISCs.

Unless otherwise noted, two-way ANOVA followed by Sidak's multiple comparisons tests were used for statistical analysis and n = number of midguts/flies. a.u., arbitrary units. Data are represented as mean ± SD. ns, not significant; $^{**}p < 0.01$, $^{****}p < 0.0001$. Scale bars, 50 μm.

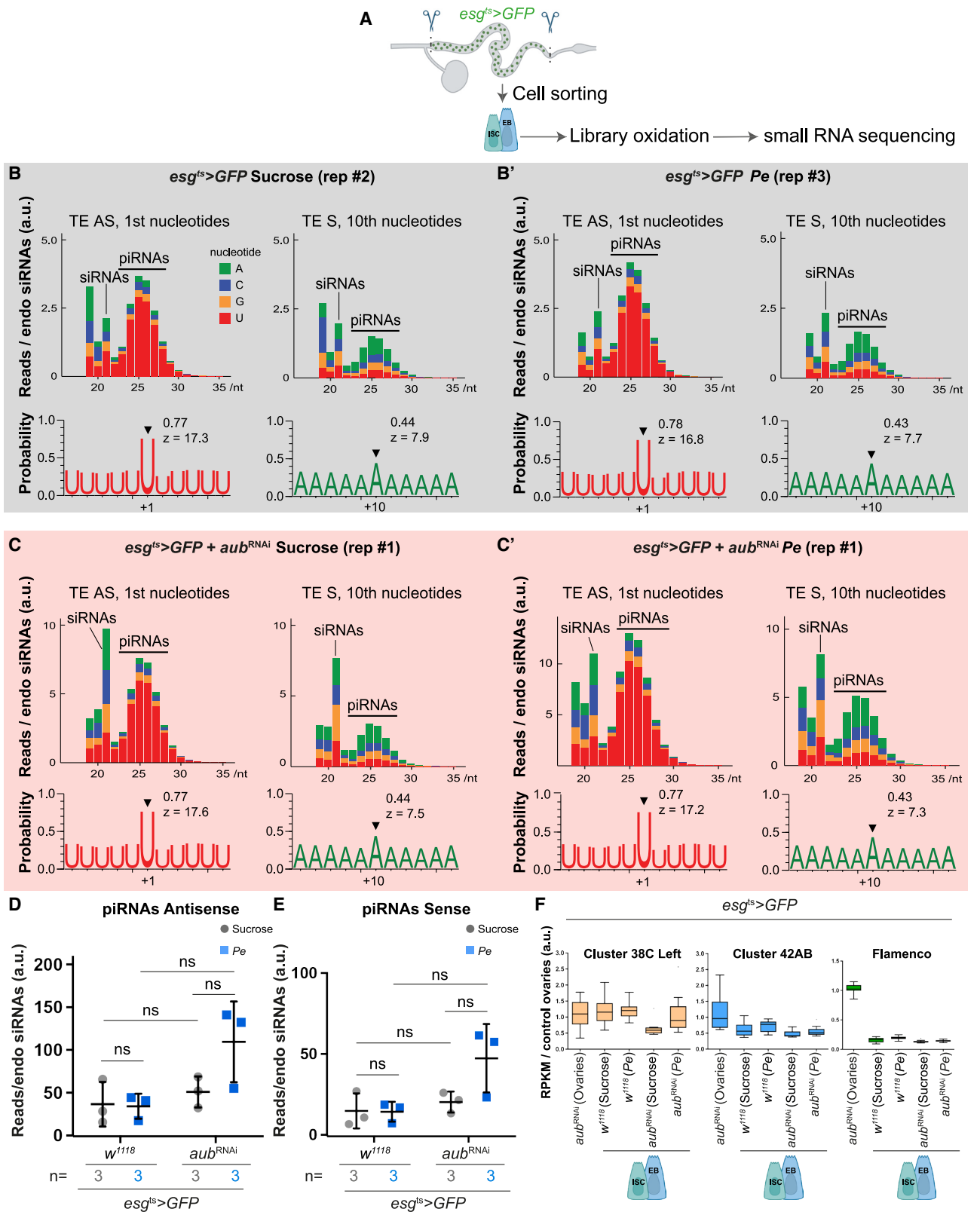

(legend on next page)

proliferation.[50] To distinguish the cell type where *aub* functions to regulate ISC proliferation, we induced gene knockdown in EBs or ISCs only using cell-specific drivers *Su(H)GBE-Gal4,UAS-GFP; tub-Gal80^{ts}* or *esg-Gal4,UAS-GFP; Su(H)GBE-Gal80, tub-Gal80^{ts}*, respectively (hereafter referred to as *EB^{ts}* and *ISC^{ts}*, respectively; Figures 1K and 1L).[51,52] While no impact on intestinal regeneration was observed upon knocking down *aub* in EBs (Figure 1K), gene knockdown in ISCs was sufficient to recapitulate the impairment in regeneration observed upon dual ISCs/EBs *aub* knockdown (Figure 1L). Collectively, these results suggest that the role of Aub in midgut regeneration is ISC autonomous (Figure 1M). Consistently, Aub knockdown did not affect the production of the EB-derived Wg (Figures S1K–S1M).

Midgut stem/progenitor cells express TE mapping piRNA-like small RNAs, which are not affected upon *aub* knockdown

The fact that other key components of the piRNA amplification/ping-pong pathway did not mimic the observed *aub* phenotype (Figures 1C and S1A) led us to hypothesize that Aub may be working in a non-canonical fashion to induce regenerative ISC proliferation in the adult midgut. Next, we took multiple complementary approaches to understand the mechanisms of action of Aub in the adult *Drosophila* midgut.

The presence of 2′-*O*-methylation at the 3′ ends of piRNAs confers resistance to sodium periodate oxidation.[9,53–55] Consequently, RNA samples can be enriched with siRNAs and piRNAs versus other, and potentially more abundantly present, small RNA populations. Although much less prominent than in oxidized libraries from ovaries, oxidation of whole gut libraries revealed an enrichment of 23–28 nucleotides long TE antisense small RNAs (Figures S2A–S2C). Importantly, those RNAs showed nucleotide biases characteristic of piRNAs: uridines at the 1st base position of TE antisense reads (AS) and, to a lesser extent, adenines at the 10th base position of TE sense reads (S)—hallmarks of ping-pong piRNA biogenesis.[6] Notably, this enrichment was not visible in previously published unoxidized midgut libraries[28,56] (Figure S2D), emphasizing the importance of library oxidation to observe small enrichments in piRNAs. Stem/progenitor cells are underrepresented in bulk midgut tissue preparations, which include heterogeneous cellular sub-types from the intestinal epithelium and associated microenvironment (Figure 1A'). We therefore next performed small RNA sequencing of oxidized samples from sorted ISCs/EBs (Figure 2A). Compared to whole midgut samples, small RNA sequencing from ISCs/EBs of control and regenerating midguts consistently showed a more pronounced piRNA signature (Figure 2B-C′ vs. S2A and S2B). However, this was not reduced by cell-specific knockdown of *aub* (Figures 2B–2E).

Our analysis shows that as in ovaries, around 90% of all piRNA-like reads in ISCs/EBs mapped to TE sequences (Figure S2E). We also find a strong bias (around 50%) toward 'U' at the immediate downstream nucleotide position of TE and non-TE mapping reads for all libraries, indicative of phased piRNA production (Figures S2F–S2H).[18] Despite these commonalities, ISCs/EBs appear to express piRNA-like populations, distinct from those expressed in the ovaries. The tiles analysis of genome-unique piRNA mappers in ISCs/EBs versus those in ovaries showed that piRNA germline-expressed clusters 38C and 42AB are comparatively more abundant in ISCs/EBs than those from the somatic cluster *flamenco* (Figure 2F). This is consistent across all conditions and genotypes analyzed (Figures S3A–S3E). In summary, our oxidized libraries from sorted adult midgut ISCs/EBs detected small RNAs with a molecular signature consistent with that of piRNAs. However, while effective to block regenerative ISC proliferation, RNAi-dependent *aub* knockdown is not sufficient to deplete ISC/EB piRNA-like small RNAs.

Aub regulates intestinal regeneration independently of its canonical piRNA regulatory function

We next performed mRNA sequencing from sorted ISCs/EBs (Figure S3F) to measure the abundance of TE mRNAs in homeostasis and regeneration (Figures S3G and S3H). While several TEs, such as *copia*, *roo*, and *Doc*, were abundantly expressed in ISCs/EBs in both conditions, this was independent of Aub (Figures S3G and S3H). These TEs are neither abundantly expressed nor under the control of Aub in the ovaries (Figure S3I).[57] Interestingly, we observed that *flea* expression, a TE regulated by Aub in the germline,[58] (Figure S3I) was upregulated in ISCs/EBs upon *Pe* infection regardless of Aub presence (Figures S3G and S3H). These data confirm the distinctive nature of midgut vs. ovary TEs and are consistent with recent work suggesting that stress-associated TE regulation in the midgut may be carried out by mechanisms independent of the piRNA machinery.[56]

Next, we used site-directed transgenesis to generate *UAS-aub^{WT}*, *UAS-aub^{AA}*, or *UAS-aub^{ADH}* lines (Figure S4A). *UAS-aub^{AA}* contains a double point mutation in the PAZ domain, responsible for the loading of piRNAs,[59] while *UAS-aub^{ADH}* carries a single mutation in the PIWI domain, responsible for Aub's endonuclease activity and piRNA biogenesis.[19] Mutations in *aub* have been previously correlated with female sterility, a reduced size of the ovaries, and embryonic lethality.[19,42,59,60] Consistent with previous reports,[19] we observed that only

Figure 2. Aubergine does not impact the presence of piRNAs in *Drosophila* intestinal stem/progenitor cells

(A) Schematic of sorted ISCs/EBs (green dots) used for small RNA sequencing.

(B–C′) Size distribution (top) of all transposon-mapping reads and uridine and adenine frequencies of piRNA size (>22 nt) (bottom) transposon-mapping reads in oxidized libraries from sorted ISCs/EBs.

(D and E) Quantification of TE antisense (D) and sense (E) piRNAs abundance as in (B–C'). Two-way ANOVA followed by Sidak's multiple comparisons tests were applied. $n = 3$ biological replicates.

(F) Representation of piRNA clusters expression in sorted ISCs/EBs as in (B–C′), compared to ovaries.

Results are presented relative to control ovaries. a.u., arbitrary units. TE, transposable element; AS, antisense; S, sense. ns, not significant. Data are represented as mean ± SD.

UAS-aub^{WT} could partially restore fertility when expressed in the germline (Figure S4B). On the other hand, comparable levels of transgene expression in midgut ISCs/EBs (Figures S4C–S4G) were similarly capable of improving regenerative ISC proliferation in *aub*$^{HN2/QC42}$ midguts (Figure 3A) and resulted in comparable gain-of-function phenotypes in undamaged, wild-type midguts (Figures 3B and 3C). Our results suggest that Aub is necessary and sufficient to drive ISC proliferation in the adult *Drosophila* midgut, and it does so independently of its canonical piRNA regulatory function.

Aub regulates ISC proliferation through the translation of core regenerative factors in the adult midgut

To further characterize the processes underpinning the role of Aub in the midgut, we assessed its effect on regenerative signaling pathways. The EGFR/MAPK, Wnt, and JAK-STAT pathways drive intestinal regeneration through ISC activation of their respective effectors, Sox21a, Myc, and Socs36E.[41,49,50,61–66] We hypothesized that these transcription factors would represent good candidates to mediate the cell autonomous function of Aub within ISCs (Figures 1K–1M). Consistent with prior reports,[41] our RT-qPCR analysis showed upregulation of the transcriptional target of JAK/Stat signaling, *socs36e*, in sorted ISCs/EBs from *Pe*-treated midguts, confirming the regenerative status of our sorted cell population (Figure 3D). However, we observed no significant impact of *aub* knockdown on *socs36e* mRNA. In contrast, *sox21a* and *myc* mRNA expression in sorted cells did not change upon *Pe* infection and was overall increased—albeit not statistically significantly—in Aub-depleted ISCs/EBs (Figure 3D). Neither of these scenarios explained Aub-dependent ISC proliferation upon damage.

Biological functions of Aub in the germline and embryo include control of the translation of mRNAs coding for specific factors.[43,67–70] Puromycin incorporation experiments to measure global protein translation,[71–73] showed a significant increase in protein synthesis in regenerating midguts, which was highly dependent on *aub* expression (Figures 3E-G). Consistent with prior reports,[50,74] we observed significant Sox21a (Figure 3H, H′) and Myc (Figure 3I, I′) protein upregulation in ISCs during midgut regeneration. Critically, this was significantly impaired upon *aub* knockdown (Figure 3H-I′).

The preservation of proteostasis, the balance between protein synthesis and degradation, is an important aspect of intestinal homeostasis in the *Drosophila* midgut.[75] Levels of Sox21a and Myc are dynamically regulated during damage-induced ISC proliferation and post-damage recovery, with a significant decay of both proteins observed 24 h after removal of the damaging agent (Figures S5A and S5C). However, overexpression of Aub did not prevent Sox21a or Myc downregulation after damage (Figures S5B and S5D).

Knocking down the *proteasome β5* subunit (*prosβ5*)[76] in ISCs/EBs to inhibit protein degradation leads to the accumulation of multi-ubiquitinated proteins in damaged midguts (FiguresS5E and S5F). We reasoned that an increase in protein degradation upon *aub* knockdown would become evident by blocking the proteasomal machinery. However, we observed no significant difference in the levels of accumulated multi-ubiquitinated proteins upon *aub* knockdown (FiguresS5E and S5F), suggesting that Aub is not a major regulator of protein stability within ISCs during midgut regeneration.

We next assessed the capacity of *UAS-aub*^{WT}, *UAS-aub*^{AA} or *UAS-aub*^{ADH} to regulate Sox21a and Myc expression in the midgut. Overexpression of either isoform of Aub was similarly sufficient to induce mild levels of Myc and Sox21a in homeostatic wild type midguts (Figures 4A–4C) and to significantly restore protein upregulation in *aub*$^{HN2/QC42}$ midguts following pathogen-induced damage (Figures 4D–4F). Altogether, these data suggest that Aub drives regenerative ISC proliferation through cell autonomous upregulation of protein synthesis, including inducing *sox21a* and *myc* translation, either directly or indirectly and in a manner that is independent of its association with piRNAs (Figure 4G).

Aub regulates ISC proliferation through selective interaction with subunits of the translation initiation machinery

Previous studies showed that Aub promotes translation of key developmental genes in the germline by interacting with translation initiation complexes eukaryotic initiation factor complex 3 (eIF3) and 4 (eIF4).[69,70] Immunostaining revealed significant upregulation of eIF3C (Figures 5A, 5B, and S6A) and eIF4G (Figures 5C, 5D, and S6B) subunits in ISCs/EBs in response to damage.

Next, we measured regenerative ISC proliferation upon RNAi-dependent knockdown of *eIF3* and *eIF4* subunits *eIF3C*, *eIF3M*, *eIF3G*[77,78], and *eIF4G*, a previously known binding partner of Aub in the germline (Figure 5E).[69] Experiments on *eIF3B*, *eIF3D*, *eIF4A*, and *eIF4E* knockeddown did not progress due to high animal lethality or homeostatic ISC loss. Among the factors whose depletion did not affect ISCs homeostasis, RNAi against *eIF3C* and *eIF3M* impaired ISC proliferation upon infection or Aub overexpression. In contrast, RNAi against *eIF3G* and *eIF4G* did not impact regenerative ISC proliferation or only affected damage-induced ISC proliferation while having minimal impact on Aub-induced ISC proliferation (Figures 5E–5G).

Consistent with its impact on regenerative (Figures 5E and H) and Aub-induced ISC proliferation (Figure 5G), knocking down *eIF3M* significantly impaired protein translation (Figures 5I and 5J) and the upregulation of Sox21a and Myc following midgut damage (Figures 5K–5N, and S6E–S6H). Interestingly, while *eIF3c* knockdown efficiently inhibited protein translation (Figures S6C and S6D), intestinal regeneration (Figure 5E), and Aub-induced ISC proliferation (Figure 5F), it did not show detectable impact on damage-induced upregulation of either Sox21a or Myc in ISCs (Figures 6A–6D), suggesting that unidentified targets of eIF3C, other than Sox21a and Myc, promote its role in regenerative and Aub-dependent ISC proliferation. Further investigation into the relationship between Aub and eIF3C revealed that the observed upregulation of eIF3C upon midgut damage (Figures 5A and 5B) was post-transcriptional (Figure 6E) and dependent on Aub (Figures 6F–6H). Notably, Aub knockdown did not affect eIF4G induction (Figures S6I and S6J). Overall, these results indicate a functional link between Aub and eIF3C that does not globally extend to core translation initiation factors. Furthermore, they point to a selective rather than general role of Aub regulating protein translation in the regenerating

CellPress
OPEN ACCESS

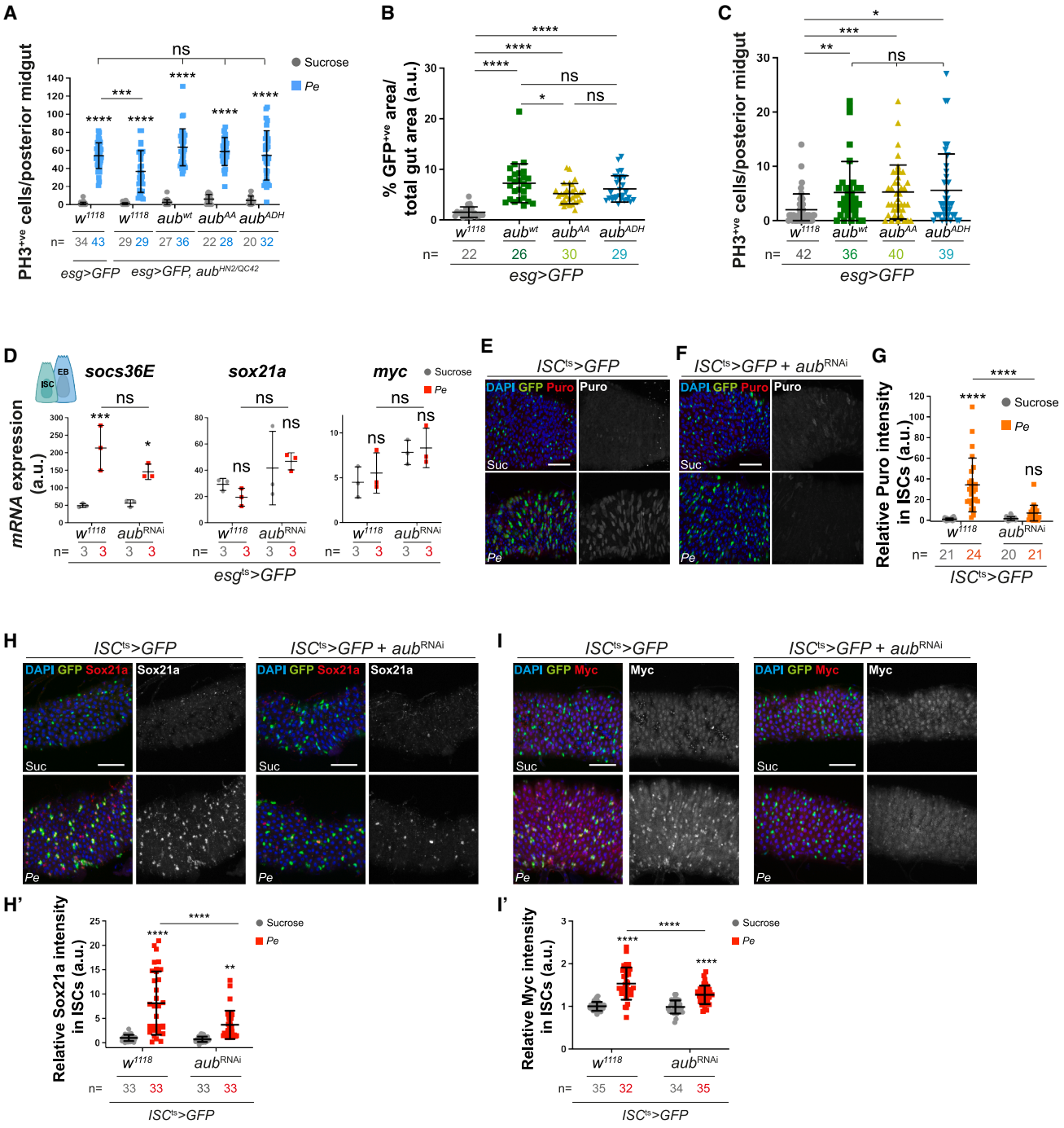

Figure 3. Aub regulates intestinal regeneration independently of its piRNA regulatory function

(A) PH3-positive cells in aub^{HN2}/aub^{QC42} midguts expressing GFP alone or with aub^{WT}, aub^{AA}, or aub^{ADH} within ISCs/EBs.

(B) *esg>GFP* area in control ISCs/EBs or overexpressing aub^{WT}, aub^{AA}, or aub^{ADH}. Shapiro-Wilk normality test followed by Mann-Whitney *t* test.

(C) PH3 cells in midguts as in B. Shapiro-Wilk normality test followed by a Kruskal-Wallis one-way ANOVA and Dunn's multiple comparisons test.

(D) Relative mRNA expression of *socs36e*, *sox21a*, and *myc* in sorted ISCs/EBs. *n* = 3 biological replicates.

(E and F) Puromycin staining (red and gray) in control ISCs (green) or expressing aub^{RNAi}.

(G) Quantification of data in (E) and (F).

(H and I) Sox21a (H) and Myc (I) staining (red and gray) in control ISCs (green) or expressing aub^{RNAi}. (H′ and I′) Quantification of data in (H) and (I).

Unless otherwise noted, two-way ANOVA followed by Sidak's multiple comparisons tests were applied. n = number of midguts/flies quantified. a.u., arbitrary units. ns, not significant; *$p < 0.05$, **$p < 0.01$, ***$p < 0.001$, and ****$p < 0.0001$. Data are represented as mean ± SD. Scale bars, 50 μm.

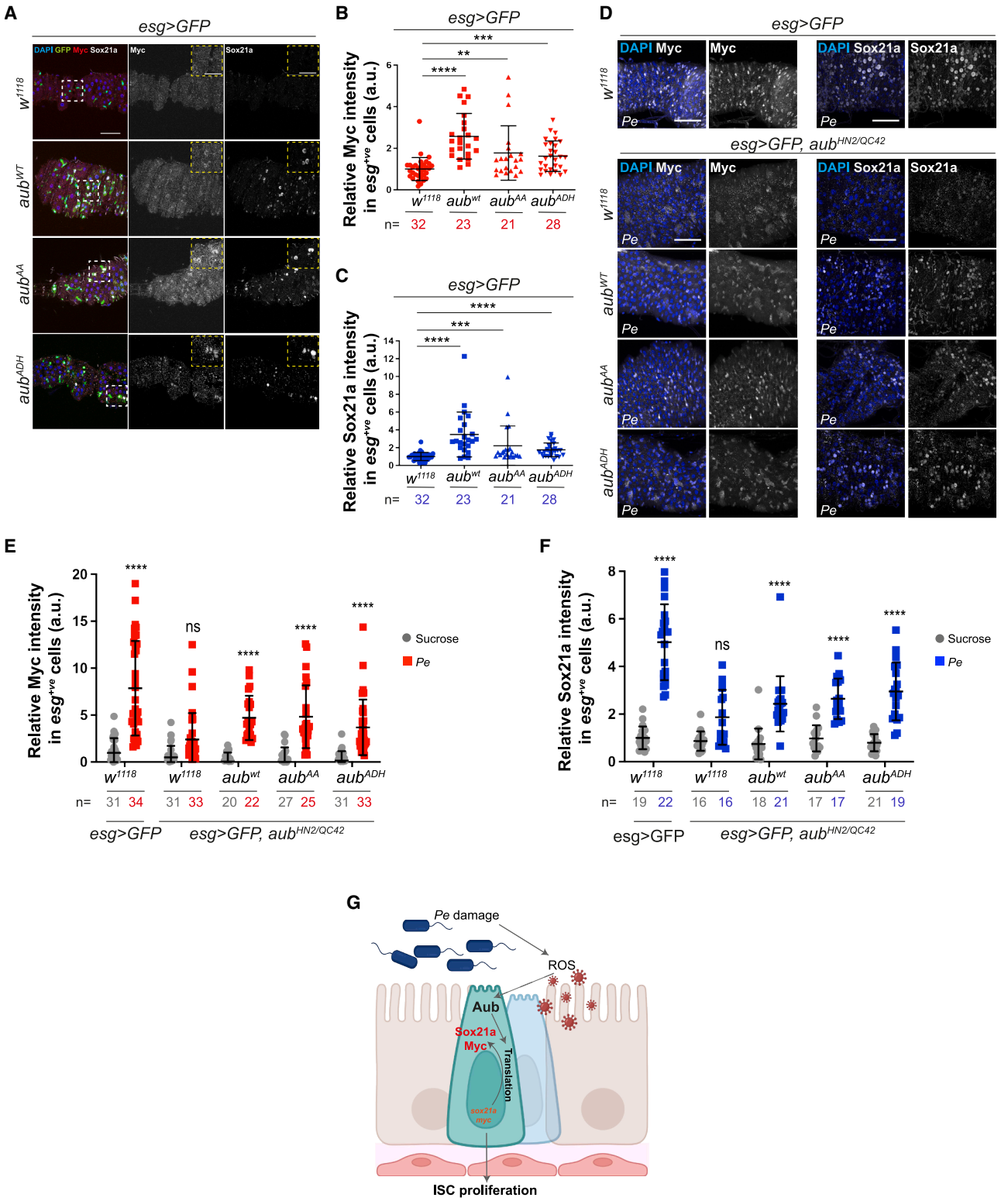

Figure 4. Aub regulates core regenerative stem cell factors in the adult midgut

(A) Myc and Sox21a staining in ISCs/EBs from control flies or flies overexpressing *aub*^{WT}, *aub*^{AA}, or *aub*^{ADH}. Dashed white squares delineate magnified areas shown in the dashed yellow panels.

(legend continued on next page)

midgut. Consistently, knocking down *aub* had no effect on the upregulation of Armadillo/β-Catenin (Figures S6K and S6L), a conserved component of canonical Wnt signaling, that regulates gene transcription, including Myc, during intestinal regeneration and cancer.[79,80] This suggests that Aub activate Myc expression downstream of Armadillo/β-Catenin.

Altogether, these results suggest that Aub regulates regenerative ISC proliferation by inducing, directly or indirectly, the translation of a subset of mRNAs, including *sox21a*, *myc*, and *eIF3C* (Figures 6I and 6J). Furthermore, the role of Aub in ISCs involves functional interaction with specific subunits of the translation initiation complex.

Aub and PIWIL1 drive ISC proliferation in CRC

Growing evidence in humans suggests misexpression of PIWI proteins and/or piRNAs in multiple cancers,[81–91] including colorectal[92–95] and gastric cancers.[82,96] We used a PIWIL1 antibody (Figures S7A and S7B) to stain tissue samples from CRC patients, which showed strong expression of cytoplasmic PIWIL1 in tumor tissue from advanced stage cancers (Figure S7C). Consistently, our analysis of *PIWIL1* gene expression in colon tissue samples revealed significantly higher *PIWIL1* gene expression in colon adenocarcinoma versus normal tissues (Figures 7A and 7B). Microarray data analysis revealed strong overexpression of *PIWIL1* in aggressive metastatic colon tumors (Figure 7C). Analysis of *PIWIL1* expression across different CRC subtypes,[97] showed *PIWIL1* gene expression significantly upregulated in the consensus molecular subtype 1 (CMS1) human CRC subtype (Figure 7D), which presents high microsatellite instability correlated with hypermethylated profiles and strong immune activation.[97] Consistently, we observed significant *PIWIL1* upregulation in patients with tumors characterized by high microsatellite instability (Figure 7E).

Survival analysis from a large local cohort of CRC patients demonstrated a significant association between high *PIWIL1* RNA expression and reduced cancer specific survival only in patients with stage 3 disease (Figures 7F and S7D, and S7E), which was potentiated in patients with rectal tumors (Figure 7G). Altogether, our results confirm a positive correlation between *PIWIL1* and CRC and identify specific CRC subtypes where *PIWIL1* overexpression is most prominent, suggesting potential selectivity in the role of *PIWIL1* toward highly aggressive intestinal tumors.

We next looked at Aub expression in a CRC-like fly model driven by the loss of the tumor suppressor *Adenomatous polyposis coli* (*Apc*), a major driver of early intestinal tumorigenesis, whose loss leads to hyperactivation of Wnt signaling through constitutive activation of β-catenin and upregulation of Myc.[80,98,99] Aub expression was increased in ISCs/EBs from hyperplastic *Apc1* mutant midguts (Figures 7H–7J).[80,100] We next used the MARCM lineage tracing system[44] to induce ISC control (*LacZ*) or *Apc1* mutant clones upon *aub* knockdown (aub^{RNAi}; Figures 7K and 7L). While *aub* knockdown did not impact homeostatic clonal growth (Figures 7K and 7L), it strongly suppressed overgrowth of *Apc1* clones (Figures 7K and 7L) and ISC proliferation following overexpression of the Wnt ligand Wingless (Wg)[50,66,80] (Figure S7F). Together with our regeneration data, these results reinforce the essential role of ISC Aub mediating tumorigenesis downstream of Wnt ligand and β-catenin activity.

Screening a panel of human CRC organoids for *PIWIL1* expression revealed highest levels of gene expression in organoids derived from aggressive tumor types when compared to those obtained from benign polyps (Figure 7M). We used shRNA-dependent gene knockdown to address the functional role of *PIWIL1* in the two patient-derived CRC organoid lines that showed highest gene expression levels (Figures 7N and 7O). Two independent shRNA constructs showed significant *PIWIL1* knockdown, with one shRNA (*shPIWIL1-2*) leading to at least 70% gene knockdown efficiency in organoid lines (Figures S7G and S7H). Knocking down *PIWIL1* resulted in strong impairment of organoid clonogenicity/proliferative capacity (Figures 7P and 7R), and survival (Figures 7Q and 7S) without affecting organoid stemness as assessed by expression of the ISC marker *Lgr5* (Figures S7I and S7J). In line with our *Drosophila* findings, these results suggest that PIWIL1 does not impair stem cell maintenance in the intestine, but it is required to drive ISC hyperproliferation and tumor growth in human CRC organoids.

Altogether, our data suggest a stem cell intrinsic role of Aub inducing intestinal regeneration and tumorigenesis and a similar function of PIWIL1 driving human intestinal tumor growth. Importantly, we provide *in vivo* and *in vitro* paradigms amenable for broader mechanistic studies on the role of PIWI proteins and piRNAs in intestinal physiology and tumorigenesis.

DISCUSSION

Multiple lines of evidence have demonstrated roles of PIWI proteins beyond their well-defined function as repressors of TEs expression.[43,59,67–70,101–103] Here, we present a non-canonical role of intestinal stem cell Aub, which involves the regulation of intestinal regeneration through translational control of conserved transcription factors and a core subunit of the translation initiation machinery.

An inducible source of aub regulates ISC proliferation in the regenerating adult *Drosophila* midgut

While levels of *aub* mRNA expression in the midgut are very low when compared to ovaries, pathogenic stress leads to striking upregulation of Aub protein in regenerating midguts (Figure 1). Remarkably, this upregulation extends to exogenous overexpressed Aub coding sequences with minimal mRNA translation domains (Figure S4), suggesting a likely post-translational mechanism regulating Aub in the system. We identified ROS as a

(B and C) Quantification of Myc (B) and Sox21a (C) staining as in (A). Shapiro-Wilk normality test followed by Mann-Whitney *t* test.
(D) Myc and Sox21a staining in ISCs/EBs from aub^{HN2}/aub^{QC42} midguts expressing aub^{WT}, aub^{AA}, or aub^{ADH} in ISCs/EBs.
(E and F) Quantification of staining as in (D). Two-way ANOVA followed by Sidak's multiple comparisons test. n = number of midguts/flies. a.u., arbitrary units.
(G) Schematic of Aub regulation and its function on Sox21a and Myc induction in regenerating ISCs. Data are represented as mean ± SD. ns, not significant ($p > 0.05$), *$p < 0.05$, **$p < 0.01$, ***$p < 0.001$, and ****$p < 0.0001$. Scale bars, 50 μm.

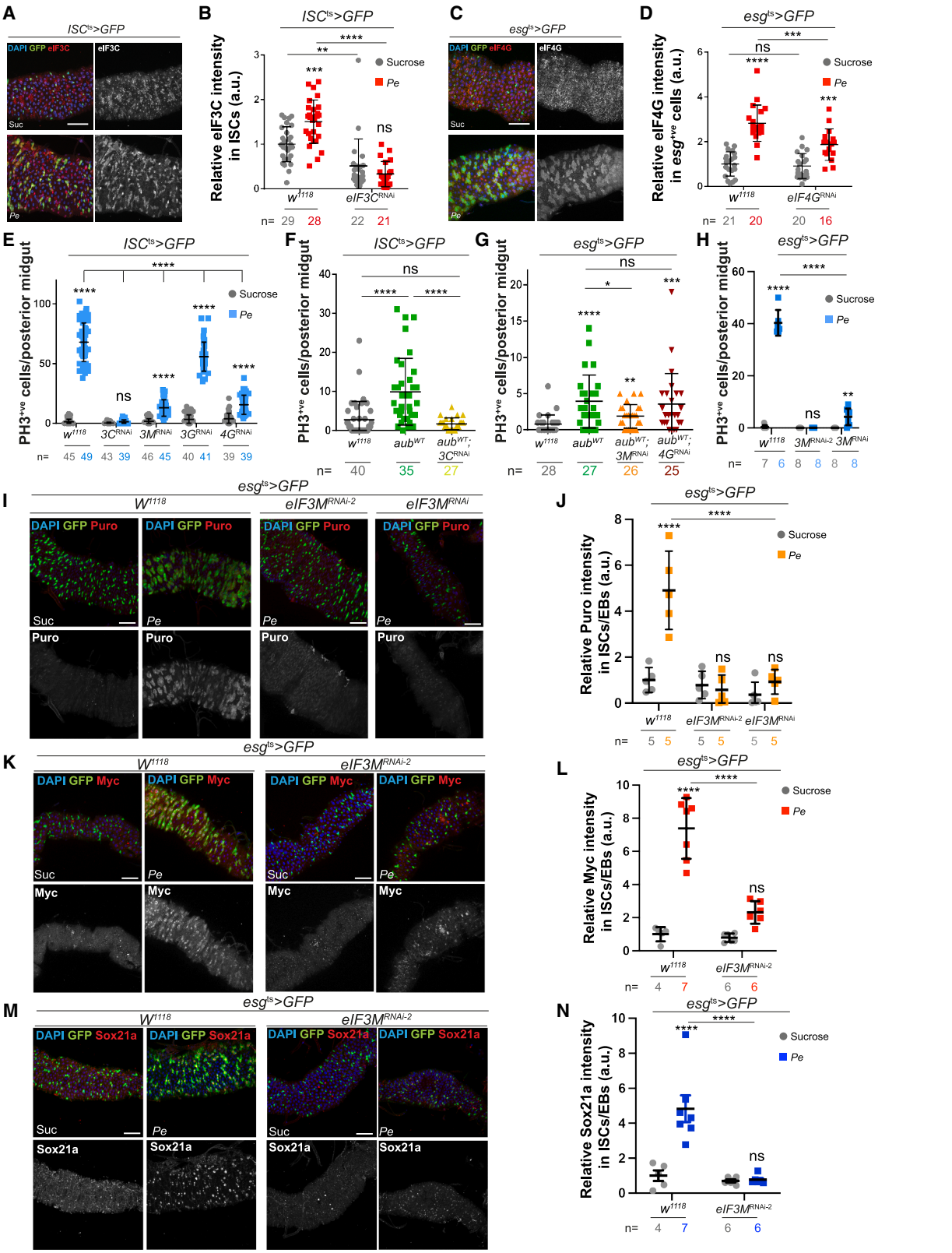

(legend on next page)

regulator of damage-induced Aub in the regenerating midgut (Figure 1). A conserved role of ROS on transcriptional and post-translational regulation of HIF1-α/Sima[47,104] is associated with its influence in the remodeling of the vascular microenvironment of the regenerating midgut.[47] As such, one possibility is that ROS may preserve Aub protein stability during intestinal repair.

Aub acts as a regulator of protein translation in ISCs

Our work underscores a central role of inducible protein synthesis in the capacity of stem cells to trigger the regenerative response of the intestine following damage, as well as the complexity of the protein translation machinery operating within ISCs.

Results from our puromycin incorporation assay suggest that upregulation of protein translation is a prominent feature of the regenerative response of ISCs to damage and that Aub is required for a significant proportion of such response, including translation of key regeneration effector proteins, such as Sox21a and Myc. Questions emerging from our study include: is damage-induced regeneration in general and Aub in particular linked to upregulation of global or mRNA specific translation? What are the mechanisms of translation employed by regenerating ISCs?

Our data only partially address some of these questions. On the one hand, the striking inhibitory effect of Aub knockdown on puromycin incorporation and its necessity to upregulate the expression of the core translation initiation factor subunit eIF3C may indicate a non-discriminatory role of Aub on global protein translation. However, we showed that knockdown of eIF3C is not sufficient to impair translation of the two Aub targets *sox21a* and *myc* Figure 6). Furthermore, Aub knockdown does not impair the upregulation of two highly relevant drivers of regenerative ISC proliferation, eIF4G and Arm/β-Catenin (Figure S6). This evidence suggests that, rather than global, the role of Aub on protein translation in regenerative ISCs is likely to involve the regulation of specific subsets of mRNAs.

While canonical mRNA translation involves assembly of the complete translation initiation machinery,[105] differential requirement of translation initiation factors and target specific mRNA translation by the eIF3 and eIF4 have been reported in *Drosophila* and mice.[77,106–108] Consistently, our results show that eIF3C likely drives ISC proliferation upon damage through the regulation of a yet to be identified subset of mRNAs. On the other hand, the non-core eIF3M subunit induces broad protein translation, including Sox21a and Myc, in regenerating ISCs.

Physical interaction with target mRNAs or translation initiation factor subunits mediates the role of Aub in post-transcriptional gene regulation in the germline and ovaries.[69,70] Unbiased molecular and biochemical approaches for global analysis of protein/protein and protein/RNA interactions will be needed to fully understand the translatome and composition of the translational machinery of regenerating ISCs, and the molecular mechanism mediating the role of Aub in mRNA translation in the midgut.

Aub and PIWIL1 in colorectal cancer

Our observations suggest that the upregulation of Aub is a common feature of regenerative and oncogenic ISC hyperproliferation. Alterations of the protein translation machinery are a cancer hallmark.[109] Over 95% of human CRC cases bear loss-of-function mutations in the tumor suppressor *APC*, leading to Wnt pathway hyperactivation and the subsequent upregulation of its target gene *myc*.[110] Myc expression in CRC relies on the activity of the eukaryotic initiation factor eIF4E[111,112] and eIF4A1,[113] two factors that, when knocked down, resulted in strong homeostatic stem cell loss in our studies (not shown). Furthermore, eIF3M expression is functionally linked to increased cell proliferation in human colorectal cancer cell lines.[114] It is therefore possible that the mechanisms mediating the upregulation and proliferative function of Aub in intestinal regeneration may extrapolate to the regulation and function of Aub and PIWIL1 in tumors. Our work presents excellent paradigms to address these questions.

Aub functions independently of piRNAs in ISCs of the adult *Drosophila* midgut

Given that Aub is considered essential for ping-pong piRNAs biogenesis in the germline, our results suggesting its dispensability for the synthesis of the identified ping-pong piRNA-like signature in ISCs were unexpected (Figure 2). Detecting a trace amount of contaminated RNA from ovaries, which were not subject to RNAi knockdown in our system, is unlikely because both TE mRNAs and cluster-derived piRNAs are differentially represented in the sorted ISC/EBs compared to ovaries (Figures S2 and S3). Instead, this could be explained by either sufficiency to

Figure 5. Aub interacts with selective eIF3 subunits to regulate ISC function during midgut regeneration

(A) eIF3C staining (red and gray) in ISCs (green).
(B) Quantification of eIF3C staining as in (A) and upon *eIF3c* RNAi overexpression in ISCs.
(C) eIF4G staining (red and gray) in ISCs/EBs (green).
(D) Quantification of eIF4G staining in midguts as in (C) and upon *eIF4G* RNAi overexpression in ISCs/EBs.
(E) PH3 in midguts expressing RNAi against eIF3 complex subunits or eIF4G within ISCs.
(F) PH3-positive cells in midguts expressing aub^{WT} or aub^{WT} with $eIF3C^{RNAi}$ within ISCs. Shapiro-Wilk normality test followed by a Kruskal-Wallis one-way ANOVA and Dunn's multiple comparisons test.
(G) PH3-positive cells in midguts expressing aub^{WT} or aub^{WT} with $eIF3M^{RNAi}$ or $eIF4G^{RNAi}$ within ISCs/EBs. Shapiro-Wilk normality test followed by Mann-Whitney *t* test.
(H) PH3 in midguts expressing independent $eIF3M^{RNAi}$ lines in ISCs/EBs.
(I) Puromycin staining (red and gray) in ISCs/EBs (green) of midguts as in (H).
(J) Quantification of data as in (I).
(K and M) Myc (K) and Sox21a (M) staining (red and gray) in ISCs/EBs (green) expressing GFP or $eIF3M^{RNAi-2}$.
(L and N) Quantification of staining as in (K) and (M), respectively.
Unless otherwise noted, two-way ANOVA followed by Sidak's multiple comparisons tests were applied. n = number of midguts/flies. a.u., arbitrary units. Data are represented as mean ± SD. ns, not significant; $^{*}p < 0.05$, $^{**}p < 0.01$, $^{***}p < 0.001$, and $^{****}p < 0.0001$. Scale bars, 50 μm.

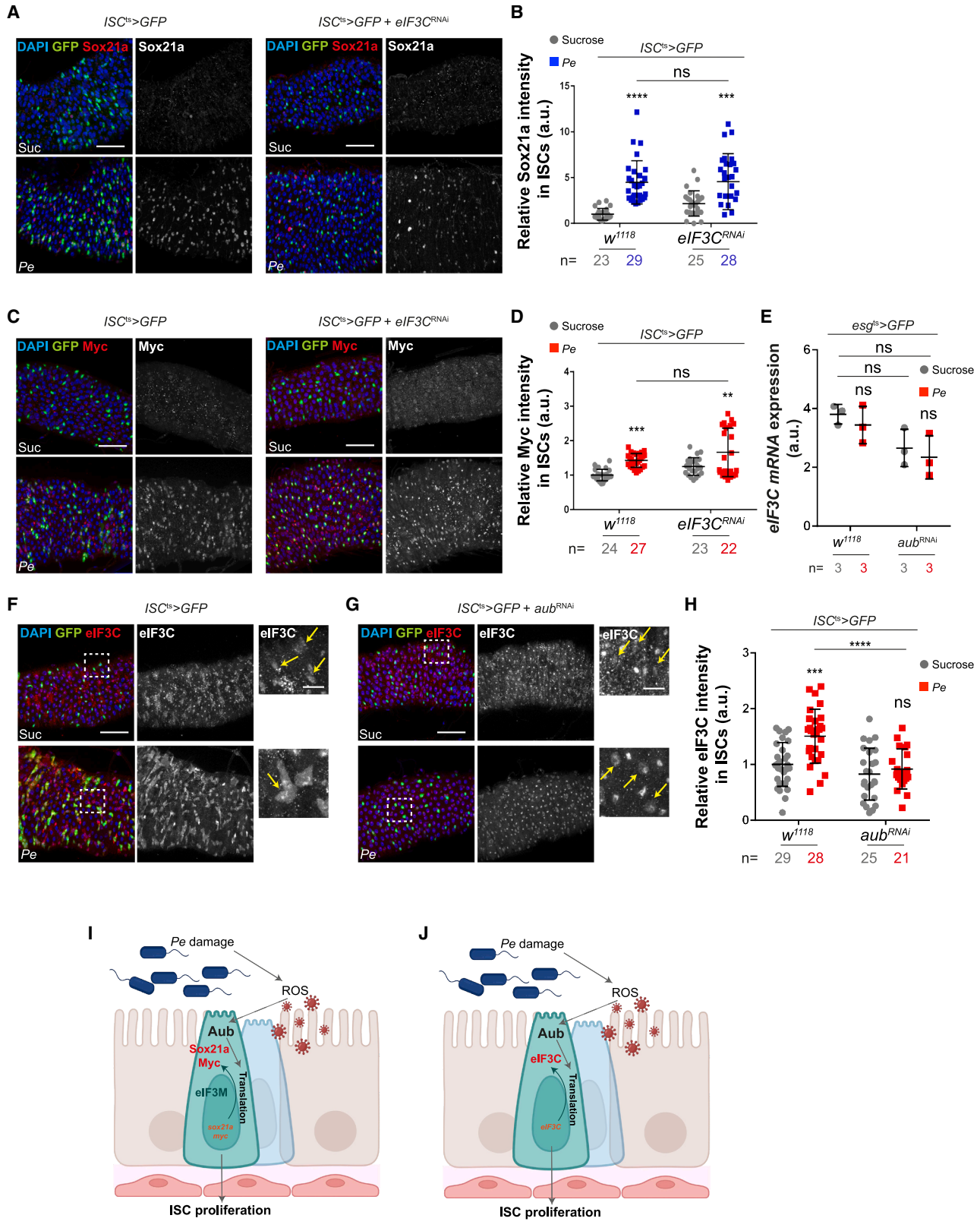

(legend on next page)

regulate piRNA with residual levels of Aub expected from RNAi partial gene knockdown or by a non-canonical Piwi- an Ago3-dependent regulation of ISC ping-pong piRNAs in the absence of Aub. Alternatively, Aub and Ago3 may work redundantly in ping-pong piRNAs biogenesis in the midgut. Redundant roles of Aub and Ago3 have been reported in the germline.[57] As such, it would be highly important that work focusing on the regulation and function of piRNAs in ISCs addresses a potential functional role of Ago3 on its own or redundantly with Aub.

Beyond its role in transposon silencing, Aub has been implicated in several non-canonical processes, including mRNA translation, localization, and degradation.[43,59,69,102,115] In the female germline, Aub regulates the translation of developmental mRNAs to promote stem cell self-renewal and differentiation.[43,69] Interestingly, Rojas-Ríos et al. found that the Aub-binding site in *cbl* mRNA closely matches one of the transposon-targeting piRNAs,[43] whereas Ma et al. reported that Aub iCLIP peaks in more than 1,000 mRNAs showed no sequence homology to piRNAs.[69] Notably, recent work in mice demonstrated that piRNAs can guide target cleavage even without perfect pairing in the seed region,[116] likely endowing the germline with a robust genome protection strategy against fast-evolving TEs. Although similar evidence is lacking in other species, this raises the possibility that Aub may also engage targets through a relaxed, yet still piRNA-dependent, recognition mode.

In contrast to its germline functions, our results show that the ability of Aub to promote intestinal stem cell proliferation and activate Sox21a and Myc expression in the adult midgut appears piRNA independent as it does not require the piRNA binding or cleavage domain of Aub (Figures 3, 4, and S4). This is reminiscent of PIWIL1 in pancreatic and gastric cancer, which functions independently of its piRNA-binding capacity.[82,117] However, while we find that Aub induces protein production in regenerating ISCs, described roles of PIWIL1 in pancreatic and gastric cancer involve induction of mRNA decay and protein degradation as a co-activator of UPF1 and of the anaphase-promoting complex/cyclosome, respectively.[82,117] The unifying principles underlying these non-canonical roles of Aub, and PIWI proteins more broadly, remain unclear. Nevertheless, our findings support the emerging view that PIWI proteins can acquire regulatory functions independent of piRNAs and outside the germline.

Limitations of the study

Classical studies characterizing molecular functions of piRNAs and PIWI proteins include immunoprecipitation of PIWI proteins and associated RNAs.[6,7,57]We have not been able to consistently and specifically immunoprecipitate Aub/piRNA complexes from ISCs, likely due to the low abundance of piRNA combined with insufficient amounts of immunoprecipitated Aub from intestinal stem cells when compared to ovary samples. Although the small RNAs detected in our sorted ISCs/EBs preparations showed strong piRNA-like molecular signature, it remains to be determined whether they are indeed associated with PIWI proteins and therefore fit the classical definition of bona-fide piRNAs, and how they may function in ISCs. Such limitations also precluded us from reliably identifying direct target mRNAs or protein partners of Aub in ISCs, as such experiments often require a large amount of material recovered from homogeneous cell populations.[69] Experimental models amenable for large scale production of cellular material, such as newly emerging intestinal-derived cell lines,[118] or human intestinal organoids (Figure 7), may facilitate conventional biochemical and molecular biology approaches for protein/RNA and protein/protein interaction studies focused on the role of PIWI proteins and piRNAs in the intestine.

RESOURCE AVAILABILITY

Lead contact

Requests for further information and resources should be directed to and will be fulfilled by the lead contact, Julia B. Cordero (julia.cordero@glasgow.ac.uk).

Materials availability

All unique/stable reagents generated in this study are available from the lead contact without restriction.

Data and code availability

- RNA-seq data have been deposited at GEO: GSE253621 and GEO: GSE253624 and are publicly available as of the date of publication. TempOSeq RNA-seq data from CRC patients have been deposited at NCBI: PRJNA997336 and are publicly available as of the date of publication. All numeric source data and raw imaging data related to this study have been deposited at Enlighten Research Data Repository at: https://doi.org/10.5525/gla.researchdata.2169 and are publicly available as of the date of publication.
- All original codes have been deposited on Zenodo (https://doi.org/10.5281/zenodo.18608988) and on Github (https://github.com/RippeiHayashi/gut_aubergine) and are publicly available as of the date of publication.
- Any additional information required to reanalyze the data reported in this paper is available from the lead contact upon request.

ACKNOWLEDGMENTS

We would like to thank Allison Bardin, Benoit Bîteau, Julius Brennecke, Ginés Morata, Yulii Shidlovskii, Paul Lasko, Marc Amoyel, Sebastian Rampf, Michael Marr, Matthias Hentze, and Phillip Zamore for flies and reagents; the

Figure 6. Aub interacts with selective eIF3 subunits to regulate ISC function during midgut regeneration

(A) Sox21a staining (red and gray) in ISCs expressing *eIF3C*^{RNAi} (green).
(B) Quantification of staining as in (A).
(C) Myc staining (red and gray) in ISCs expressing *eIF3C*^{RNAi} (green).
(D) Quantification of staining as in (C).
(E) Relative mRNA expression of *eIF3C* in control or *aub*^{RNAi} sorted ISCs/EBs. $n = 3$ biological replicates.
(F and G) eIF3C staining (red and gray) in ISCs expressing *aub*^{RNAi} (green; yellow arrows).
(H) Quantification of data as in (F) and (G).
(I and J) Schematic working models of the proposed interrelationship between Aub and eIF3M (I) or eIF3C (J) during regenerative ISC proliferation.
Unless otherwise noted, two-way ANOVA followed by Sidak's multiple comparisons tests were applied. n = number of midguts/flies. a.u., arbitrary units. Data are represented as mean ± SD. ns, not significant; $^{*}p < 0.05$, $^{**}p < 0.01$, $^{***}p < 0.001$, and $^{****}p < 0.0001$. Scale bars, 50 μm.

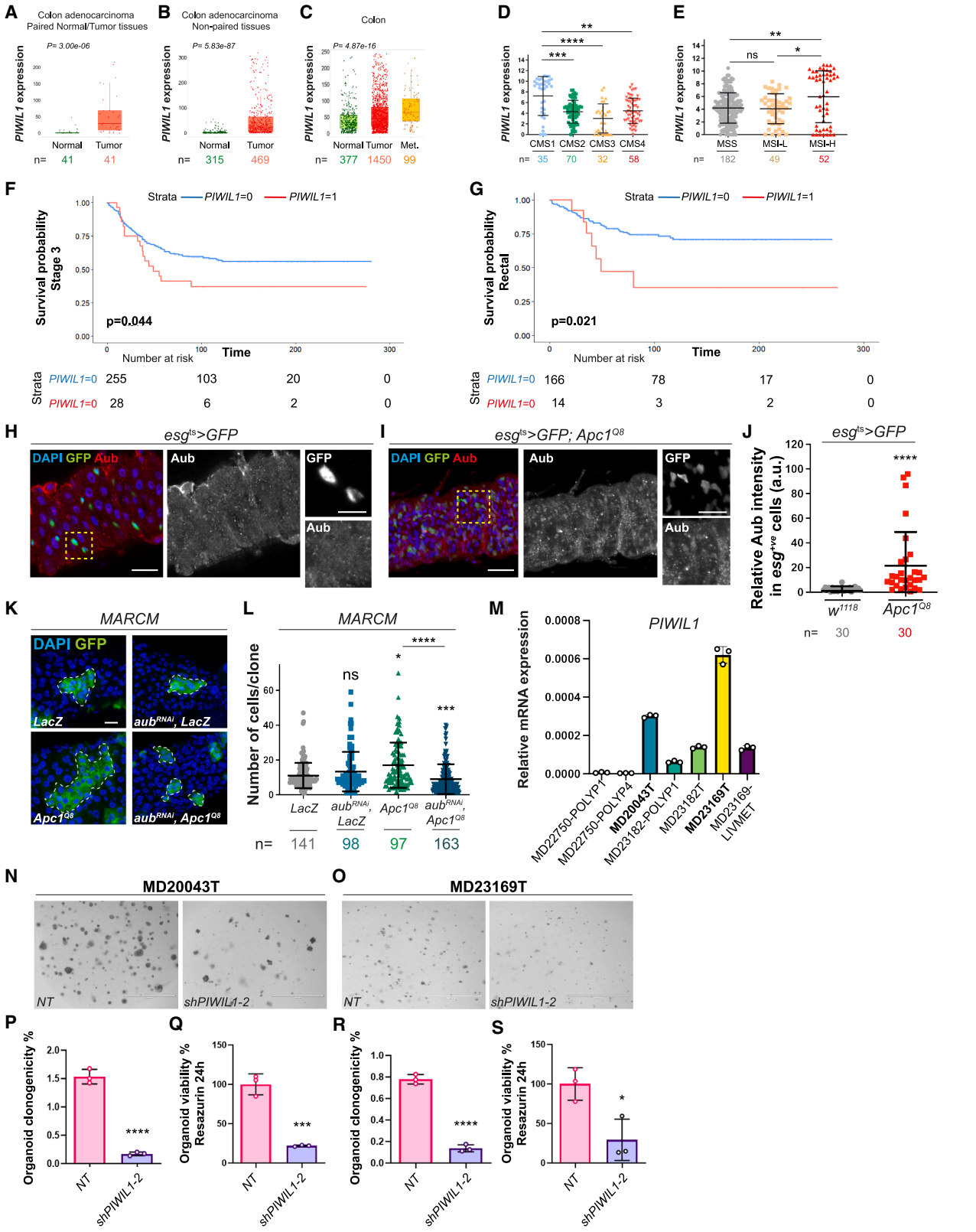

(legend on next page)

Bloomington *Drosophila* Stock Center, the Vienna *Drosophila* Resource Center, and the *Drosophila* Studies Hybridoma Bank for flies and antibodies; and the Core Services and Advanced Technologies at the CRUK Scotland Institute, which is core funded by Cancer Research UK (A31287). We give particular thanks to Leo Carlin, Claire Mitchell and Peter Thomason from the Beatson Advanced Imaging Resource, Yi-Hsia Liu and Thomas Gilbey from the FACS facility, and Colin Nixon and the Histology Laboratory for assistance with histology. We are grateful to Aurelio Teleman for general comments on the manuscript and to Henri Jasper and Pedro Sousa-Victor for help with cell sorting and mRNA sequencing of midgut ISCs/EBs. We thank all members of the Cordero laboratory for general advice on the project. We thank Donna Markie for SOCCS study coordination and patient recruitment. Human tumor sample analysis was performed on data generated by the TCGA Research Network: https://www.cancer.gov/tcga. The manuscript was critically reviewed by Catherine Winchester (CRUK Scotland 883 Institute). Graphical schematics in the manuscript were created using BioRender under license agreement UZ28NVH244.

Work in the Cordero laboratory is funded by Wellcome Trust and Royal Society (104103/Z/14/Z and 223091/Z/21/Z) to J.B.C., core Institutional funds from CRUK to the CRUK Scotland Institute (A31287), and a China Scholarship Council studentship to Y.T. (202006910022). Research in the Hayashi laboratory is supported by the Australian Research Council (DP210102385). The Edwards laboratory is funded by Chief Scientific Office grants (CSO EPD/22/13 [K.P. and J.E.] and CSO TCS/22/02 [J.E.]) and the Scottish Cancer Centre (CTRQQR-2021\100006). Research in the Myant laboratory is supported by the Medical Research Cancer (MRC; MR/X008762/1). Human organoids work was funded by the CRUK Scotland Center (CTRQQR-2021\100006) and CRUK Program Grant (DRCPGM\100012) to M.G.D. The Gontijo and Heredia laboratory was supported by the FCT (LISBOA-01-0145-FEDER-030753; 10.54499/CEECINST/00102/2018/CP1567/CT0031; 10.54499/DL57/2016/CP1457/CT0016; EXPL/BIA-BID/1524/2021; EXPL/BIA-COM/1296/2021; 10.54499/2022.03859.PTDC; 10.54499/UIDB/04462/2020; 10.54499/UIDB/00329/2020; 10.54499/LA/P/0087/2020; 10.54499/LA/P/0121/2020; LISBOA-01-0145-FEDER-022170; and UID/Multi/04462/2019).

AUTHOR CONTRIBUTIONS

K.B. designed, performed, and analyzed most of the experiments. L.R.C. initiated the project. Y.T., Y.Y., and A.R.C. contributed to *Drosophila* experimental work for the study. K.A.F.P. and J.E. provided samples, methodology, and supervision for TMA analysis. A.B.A., C.V.B., and N.D. performed and analyzed the work on human intestinal organoids. F.H. and A.M.G. generated *esg-gal4* and aub^{NH2} recombinants. F.V.N.D. and M.G.D. harvested the human tissues from patients and supervised the organoid work. J.P.B. and A.B.A. generated the human organoid lines. K.M. designed, supervised, and analyzed the work on human intestinal organoids. R.H. designed, performed, and analyzed piRNA- and mRNA-sequencing experiments and generated the Aub-GFP transgenic constructs. J.B.C. was involved in study conceptualization, design, supervision, data analysis, and funding acquisition. K.B., R.H., and J.B.C. wrote the manuscript with input from other authors.

DECLARATION OF INTERESTS

The authors declare no competing interests.

STAR★METHODS

Detailed methods are provided in the online version of this paper and include the following:

- KEY RESOURCES TABLE
- EXPERIMENTAL MODEL AND STUDY PARTICIPANT DETAILS
  - *Drosophila melanogaster* stocks rearing, maintenance, and timelines of genetic manipulations
  - Human patient information and ethics statement
  - Human patient-derived organoids (PDOs)
- METHOD DETAILS
  - Human organoid culture media and shPIWIL1 knockdown
  - Damage-induced intestinal regeneration
  - Immunohistochemistry
  - NAC treatment
  - Generation of *aub* transgenes
  - Egg laying/eclosion assay
  - Protein translation assay
  - *Drosophila* protein expression time course
  - Fluorescence-activated single-cell sorting
  - Small RNA-sequencing
  - Small RNA-sequencing analysis
  - PolyA-selected RNA-sequencing
  - PolyA-selected RNA analysis
  - RNA extraction and RT-qPCR
  - TCGA analysis
  - Samples visualization and image acquisition
- QUANTIFICATION AND STATISTICAL ANALYSIS
  - Immunofluorescence staining
  - MARCM clones
  - Transcriptional profiling of patient tissue
  - Statistics

Figure 7. Aub and PIWIL1 mediates ISC proliferation in CRC

(A and B) *PIWIL1* expression in normal and tumor tissues from human colon adenocarcinoma. Mann-Whitney *t* test. n = number of patients.
(C) *PIWIL1* expression in normal, tumor, and metastatic tissues from human colon adenocarcinoma. Kruskal-Wallis one-way ANOVA test. n = number of patients. Boxplots: line indicates median, and box represents the values included between the 25th and 75th percentiles.
(D) *PIWIL1* expression across 4 CRC subtypes. Shapiro-Wilk normality test followed by a Kruskal-Wallis one-way ANOVA and Dunn's multiple comparisons tests. n = number of patients.
(E) *PIWIL1* expression according to microsatellite status of cancers (TCGA, PanCancer Atlas). MSS, microsatellite stability; MSI-L, low microsatellite instability; MSI-H, high microsatellite instability. Shapiro-Wilk normality test followed by a Kruskal-Wallis one-way ANOVA and Dunn's multiple comparisons tests. n = number of patients.
(F and G) Kaplan-Meier survival analysis of *PIWIL1* expression in a cohort of CRC patients (n = 787) with stage 3 disease (F) and with tumors located within the rectum (G).
(H and I) Aub staining (red) in ISCs/EBs (green) from control (H) or Apc^{1Q8} mutant midguts (I). Dashed yellow squares delineate the high magnification shown in righthand panels.
(J) Quantification of staining as in (H) and (I). Shapiro-Wilk normality test followed by Mann-Whitney *t* test. n = number of cells quantified.
(K) MARCM clones (green) expressing *LacZ* (control) or in combination with aub^{RNAi} and Apc^{1Q8} clones with or without aub^{RNAi}. Dashed white lines delineate clonal margins. Scale bars, 50 μm (L) Number of cells per clone as in (K). Shapiro-Wilk normality test followed by Kruskal-Wallis one-way ANOVA and a Dunn's multiple comparisons tests. n = number of clones quantified.
(M) Relative *PIWIL1* mRNA expression in human intestinal organoids derived from polyps or from colorectal tumors. n = 3 biological replicates.
(N and O) Patient-derived CRC organoids transduced with a non-targeted control (NT) or *shPIWIL1-2* RNAi. Scale bars, 1,000 μm.
(P–S) Organoid clonogenicity upon NT or *shPIWIL1-2* RNAi transduction. Unpaired *t* tests. n = 3 biological replicates. a.u., arbitrary units. In all cases, data are represented as mean ± SD. ns, not significant; $^{*}p < 0.05$, $^{**}p < 0.01$, $^{***}p < 0.001$, and $^{****}p < 0.0001$. *LIVEMET*, liver metastasis.

SUPPLEMENTAL INFORMATION

Supplemental information can be found online at https://doi.org/10.1016/j.celrep.2026.117186.

Received: March 18, 2024
Revised: December 19, 2025
Accepted: March 9, 2026
Published: March 26, 2026

REFERENCES

1. Cox, D.N., Chao, A., Baker, J., Chang, L., Qiao, D., and Lin, H. (1998). A novel class of evolutionarily conserved genes defined by piwi are essential for stem cell self-renewal. Genes Dev. *12*, 3715–3727. https://doi.org/10.1101/gad.12.23.3715.
2. Lin, H., and Spradling, A.C. (1997). A novel group of pumilio mutations affects the asymmetric division of germline stem cells in the Drosophila ovary. Development *124*, 2463–2476. https://doi.org/10.1242/dev.124.12.2463.
3. Cox, D.N., Chao, A., and Lin, H. (2000). piwi encodes a nucleoplasmic factor whose activity modulates the number and division rate of germline stem cells. Development *127*, 503–514. https://doi.org/10.1242/dev.127.3.503.
4. Siomi, M.C., Sato, K., Pezic, D., and Aravin, A.A. (2011). PIWI-interacting small RNAs: the vanguard of genome defence. Nat. Rev. Mol. Cell Biol. *12*, 246–258. https://doi.org/10.1038/nrm3089.
5. Vagin, V.V., Sigova, A., Li, C., Seitz, H., Gvozdev, V., and Zamore, P.D. (2006). A distinct small RNA pathway silences selfish genetic elements in the germline. Science *313*, 320–324. https://doi.org/10.1126/science.1129333.
6. Brennecke, J., Aravin, A.A., Stark, A., Dus, M., Kellis, M., Sachidanandam, R., and Hannon, G.J. (2007). Discrete Small RNA-Generating Loci as Master Regulators of Transposon Activity in Drosophila. Cell *128*, 1089–1103. https://doi.org/10.1016/j.cell.2007.01.043.
7. Li, C., Vagin, V.V., Lee, S., Xu, J., Ma, S., Xi, H., Seitz, H., Horwich, M.D., Syrzycka, M., Honda, B.M., et al. (2009). Collapse of Germline piRNAs in the Absence of Argonaute3 Reveals Somatic piRNAs in Flies. Cell *137*, 509–521. https://doi.org/10.1016/j.cell.2009.04.027.
8. Aravin, A.A., Sachidanandam, R., Girard, A., Fejes-Toth, K., and Hannon, G.J. (2007). Developmentally Regulated piRNA Clusters Implicate MILI in Transposon Control. Science *316*, 744–747. https://doi.org/10.1126/science.1142612.
9. Houwing, S., Kamminga, L.M., Berezikov, E., Cronembold, D., Girard, A., van den Elst, H., Filippov, D.V., Blaser, H., Raz, E., Moens, C.B., et al. (2007). A role for Piwi and piRNAs in germ cell maintenance and transposon silencing in Zebrafish. Cell *129*, 69–82. https://doi.org/10.1016/j.cell.2007.03.026.
10. Aravin, A.A., Hannon, G.J., and Brennecke, J. (2007). The Piwi-piRNA Pathway Provides an Adaptive Defense in the Transposon Arms Race. Science *318*, 761–764. https://doi.org/10.1126/science.1146484.
11. Saito, K., Nishida, K.M., Mori, T., Kawamura, Y., Miyoshi, K., Nagami, T., Siomi, H., and Siomi, M.C. (2006). Specific association of Piwi with rasiRNAs derived from retrotransposon and heterochromatic regions in the Drosophila genome. Genes Dev. *20*, 2214–2222. https://doi.org/10.1101/gad.1454806.
12. Aravin, A., Gaidatzis, D., Pfeffer, S., Lagos-Quintana, M., Landgraf, P., Iovino, N., Morris, P., Brownstein, M.J., Kuramochi-Miyagawa, S., Nakano, T., et al. (2006). A novel class of small RNAs bind to MILI protein in mouse testes. Nature *442*, 203–207. https://doi.org/10.1038/nature04916.
13. Girard, A., Sachidanandam, R., Hannon, G.J., and Carmell, M.A. (2006). A germline-specific class of small RNAs binds mammalian Piwi proteins. Nature *442*, 199–202. https://doi.org/10.1038/nature04917.
14. Pane, A., Wehr, K., and Schüpbach, T. (2007). zucchini and squash encode two putative nucleases required for rasiRNA production in the Drosophila germline. Dev. Cell *12*, 851–862. https://doi.org/10.1016/j.devcel.2007.03.022.
15. Nishimasu, H., Ishizu, H., Saito, K., Fukuhara, S., Kamatani, M.K., Bonnefond, L., Matsumoto, N., Nishizawa, T., Nakanaga, K., Aoki, J., et al. (2012). Structure and function of Zucchini endoribonuclease in piRNA biogenesis. Nature *491*, 284–287. https://doi.org/10.1038/nature11509.
16. Ipsaro, J.J., Haase, A.D., Knott, S.R., Joshua-Tor, L., and Hannon, G.J. (2012). The structural biochemistry of Zucchini implicates it as a nuclease in piRNA biogenesis. Nature *491*, 279–283. https://doi.org/10.1038/nature11502.
17. Gunawardane, L.S., Saito, K., Nishida, K.M., Miyoshi, K., Kawamura, Y., Nagami, T., Siomi, H., and Siomi, M.C. (2007). A Slicer-Mediated Mechanism for Repeat-Associated siRNA 5′ End Formation in Drosophila. Science *315*, 1587–1590. https://doi.org/10.1126/science.1140494.
18. Han, B.W., Wang, W., Li, C., Weng, Z., and Zamore, P.D. (2015). piRNA-guided transposon cleavage initiates Zucchini-dependent, phased piRNA production. Science *348*, 817–821. https://doi.org/10.1126/science.aaa1264.
19. Wang, W., Han, B.W., Tipping, C., Ge, D.T., Zhang, Z., Weng, Z., and Zamore, P.D. (2015). Slicing and Binding by Ago3 or Aub Trigger Piwi-Bound piRNA Production by Distinct Mechanisms. Mol. Cell *59*, 819–830. https://doi.org/10.1016/j.molcel.2015.08.007.
20. Malone, C.D., Brennecke, J., Dus, M., Stark, A., McCombie, W.R., Sachidanandam, R., and Hannon, G.J. (2009). Specialized piRNA Pathways Act in Germline and Somatic Tissues of the Drosophila Ovary. Cell *137*, 522–535. https://doi.org/10.1016/j.cell.2009.03.040.
21. Ross, R.J., Weiner, M.M., and Lin, H. (2014). PIWI proteins and PIWI-interacting RNAs in the soma. Nature *505*, 353–359. https://doi.org/10.1038/nature12987.
22. Pal-Bhadra, M., Leibovitch, B.A., Gandhi, S.G., Chikka, M.R., Bhadra, U., Birchler, J.A., and Elgin, S.C.R. (2004). Heterochromatic Silencing and HP1 Localization in *Drosophila* Are Dependent on the RNAi Machinery. Science *303*, 669–672. https://doi.org/10.1126/science.1092653.
23. Brower-Toland, B., Findley, S.D., Jiang, L., Liu, L., Yin, H., Dus, M., Zhou, P., Elgin, S.C.R., and Lin, H. (2007). Drosophila PIWI associates with chromatin and interacts directly with HP1a. Genes Dev. *21*, 2300–2311. https://doi.org/10.1101/gad.1564307.
24. Huang, X.A., Yin, H., Sweeney, S., Raha, D., Snyder, M., and Lin, H. (2013). A Major Epigenetic Programming Mechanism Guided by piRNAs. Dev. Cell *24*, 502–516. https://doi.org/10.1016/j.devcel.2013.01.023.
25. Mochizuki, K., Fine, N.A., Fujisawa, T., and Gorovsky, M.A. (2002). Analysis of a piwi-related gene implicates small RNAs in genome rearrangement in tetrahymena. Cell *110*, 689–699. https://doi.org/10.1016/s0092-8674(02)00909-1.
26. Jones, B.C., Wood, J.G., Chang, C., Tam, A.D., Franklin, M.J., Siegel, E.R., and Helfand, S.L. (2016). A somatic piRNA pathway in the Drosophila fat body ensures metabolic homeostasis and normal lifespan. Nat. Commun. *7*, 13856. https://doi.org/10.1038/ncomms13856.
27. Sousa-Victor, P., Ayyaz, A., Hayashi, R., Qi, Y., Madden, D.T., Lunyak, V.V., and Jasper, H. (2017). Piwi Is Required to Limit Exhaustion of Aging Somatic Stem Cells. Cell Rep. *20*, 2527–2537. https://doi.org/10.1016/j.celrep.2017.08.059.
28. Tang, X., Liu, N., Qi, H., and Lin, H. (2023). Piwi maintains homeostasis in the Drosophila adult intestine. Stem Cell Rep. *18*, 503–518. https://doi.org/10.1016/j.stemcr.2023.01.001.
29. Rajasethupathy, P., Antonov, I., Sheridan, R., Frey, S., Sander, C., Tuschl, T., and Kandel, E.R. (2012). A Role for Neuronal piRNAs in the Epigenetic Control of Memory-Related Synaptic Plasticity. Cell *149*, 693–707. https://doi.org/10.1016/j.cell.2012.02.057.
30. Sharma, A.K., Nelson, M.C., Brandt, J.E., Wessman, M., Mahmud, N., Weller, K.P., and Hoffman, R. (2001). Human CD34+ stem cells express

the hiwigene, a human homologue of the Drosophila genepiwi. Blood *97*, 426–434. https://doi.org/10.1182/blood.V97.2.426.

31. Janic, A., Mendizabal, L., Llamazares, S., Rossell, D., and Gonzalez, C. (2010). Ectopic Expression of Germline Genes Drives Malignant Brain Tumor Growth in Drosophila. Science *330*, 1824–1827. https://doi.org/10.1126/science.1195481.
32. Micchelli, C.A., and Perrimon, N. (2006). Evidence that stem cells reside in the adult Drosophila midgut epithelium. Nature *439*, 475–479. https://doi.org/10.1038/nature04371.
33. Ohlstein, B., and Spradling, A. (2006). The adult Drosophila posterior midgut is maintained by pluripotent stem cells. Nature *439*, 470–474. https://doi.org/10.1038/nature04333.
34. Chen, J., Xu, N., Wang, C., Huang, P., Huang, H., Jin, Z., Yu, Z., Cai, T., Jiao, R., and Xi, R. (2018). Transient Scute activation via a self-stimulatory loop directs enteroendocrine cell pair specification from self-renewing intestinal stem cells. Nat. Cell Biol. *20*, 152–161. https://doi.org/10.1038/s41556-017-0020-0.
35. Zeng, X., and Hou, S.X. (2015). Enteroendocrine cells are generated from stem cells through a distinct progenitor in the adult Drosophila posterior midgut. Development *142*, 644–653. https://doi.org/10.1242/dev.113357.
36. Beehler-Evans, R., and Micchelli, C.A. (2015). Generation of enteroendocrine cell diversity in midgut stem cell lineages. Development *142*, 654–664. https://doi.org/10.1242/dev.114959.
37. Medina, A., Bellec, K., Polcowñuk, S., and Cordero, J.B. (2022). Investigating local and systemic intestinal signalling in health and disease with Drosophila. Dis. Model. Mech. *15*, dmm049332. https://doi.org/10.1242/dmm.049332.
38. Petsakou, A., Liu, Y., Liu, Y., Comjean, A., Hu, Y., and Perrimon, N. (2023). Cholinergic neurons trigger epithelial Ca2+ currents to heal the gut. Nature *623*, 122–131. https://doi.org/10.1038/s41586-023-06627-y.
39. Buchon, N., Osman, D., David, F.P.A., Fang, H.Y., Boquete, J.P., Deplancke, B., and Lemaitre, B. (2013). Morphological and molecular characterization of adult midgut compartmentalization in Drosophila. Cell Rep. *3*, 1725–1738. https://doi.org/10.1016/j.celrep.2013.04.001.
40. Marianes, A., and Spradling, A.C. (2013). Physiological and stem cell compartmentalization within the Drosophila midgut. eLife *2*, e00886. https://doi.org/10.7554/eLife.00886.
41. Jiang, H., Patel, P.H., Kohlmaier, A., Grenley, M.O., McEwen, D.G., and Edgar, B.A. (2009). Cytokine/Jak/Stat Signaling Mediates Regeneration and Homeostasis in the Drosophila Midgut. Cell *137*, 1343–1355. https://doi.org/10.1016/j.cell.2009.05.014.
42. Schüpbach, T., and Wieschaus, E. (1991). Female sterile mutations on the second chromosome of Drosophila melanogaster. II. Mutations blocking oogenesis or altering egg morphology. Genetics *129*, 1119–1136. https://doi.org/10.1093/genetics/129.4.1119.
43. Rojas-Ríos, P., Chartier, A., Pierson, S., and Simonelig, M. (2017). Aubergine and piRNAs promote germline stem cell self-renewal by repressing the proto-oncogene Cbl. EMBO J. *36*, 3194–3211. https://doi.org/10.15252/embj.201797259.
44. Lee, T., and Luo, L. (1999). Mosaic analysis with a repressible cell marker for studies of gene function in neuronal morphogenesis. Neuron *22*, 451–461. https://doi.org/10.1016/s0896-6273(00)80701-1.
45. Czech, B., Preall, J.B., McGinn, J., and Hannon, G.J. (2013). A transcriptome-wide RNAi screen in the Drosophila ovary reveals factors of the germline piRNA pathway. Mol. Cell *50*, 749–761. https://doi.org/10.1016/j.molcel.2013.04.007.
46. Morris, O., and Jasper, H. (2021). Reactive Oxygen Species in intestinal stem cell metabolism, fate and function. Free Radic. Biol. Med. *166*, 140–146. https://doi.org/10.1016/j.freeradbiomed.2021.02.015.
47. Perochon, J., Yu, Y., Aughey, G.N., Medina, A.B., Southall, T.D., and Cordero, J.B. (2021). Dynamic adult tracheal plasticity drives stem cell adaptation to changes in intestinal homeostasis in Drosophila. Nat. Cell Biol. *23*, 485–496. https://doi.org/10.1038/s41556-021-00676-z.
48. Medina, A.B., Perochon, J., Tian, Y., Johnson, C.T., Holcombe, J., Ramesh, P., Polcowñuk, S., Yu, Y., and Cordero, J.B. (2025). Neuroendocrine control of intestinal regeneration through the vascular niche in Drosophila. Dev. Cell *60*, 3085–3101.e6. https://doi.org/10.1016/j.devcel.2025.06.036.
49. Jiang, H., Grenley, M.O., Bravo, M.J., Blumhagen, R.Z., and Edgar, B.A. (2011). EGFR/Ras/MAPK signaling mediates adult midgut epithelial homeostasis and regeneration in Drosophila. Cell Stem Cell *8*, 84–95. https://doi.org/10.1016/j.stem.2010.11.026.
50. Cordero, J.B., Stefanatos, R.K., Scopelliti, A., Vidal, M., and Sansom, O.J. (2012). Inducible progenitor-derived Wingless regulates adult midgut regeneration in Drosophila. EMBO J. *31*, 3901–3917. https://doi.org/10.1038/emboj.2012.248.
51. Zeng, X., Chauhan, C., and Hou, S.X. (2010). Characterization of midgut stem cell- and enteroblast-specific Gal4 lines in drosophila. Genesis *48*, 607–611. https://doi.org/10.1002/dvg.20661.
52. Wang, L., Zeng, X., Ryoo, H.D., and Jasper, H. (2014). Integration of UPRER and Oxidative Stress Signaling in the Control of Intestinal Stem Cell Proliferation. PLoS Genet. *10*, e1004568. https://doi.org/10.1371/journal.pgen.1004568.
53. Kirino, Y., and Mourelatos, Z. (2007). Mouse Piwi-interacting RNAs are 2'-O-methylated at their 3' termini. Nat. Struct. Mol. Biol. *14*, 347–348. https://doi.org/10.1038/nsmb1218.
54. Ohara, T., Sakaguchi, Y., Suzuki, T., Ueda, H., Miyauchi, K., and Suzuki, T. (2007). The 3' termini of mouse Piwi-interacting RNAs are 2'-O-methylated. Nat. Struct. Mol. Biol. *14*, 349–350. https://doi.org/10.1038/nsmb1220.
55. Saito, K., Sakaguchi, Y., Suzuki, T., Suzuki, T., Siomi, H., and Siomi, M.C. (2007). Pimet, the Drosophila homolog of HEN1, mediates 2'-O-methylation of Piwi- interacting RNAs at their 3' ends. Genes Dev. *21*, 1603–1608. https://doi.org/10.1101/gad.1563607.
56. Siudeja, K., van den Beek, M., Riddiford, N., Boumard, B., Wurmser, A., Stefanutti, M., Lameiras, S., and Bardin, A.J. (2021). Unraveling the features of somatic transposition in the Drosophila intestine. Embo j *40*, e106388. https://doi.org/10.15252/embj.2020106388.
57. Senti, K.A., Jurczak, D., Sachidanandam, R., and Brennecke, J. (2015). piRNA-guided slicing of transposon transcripts enforces their transcriptional silencing via specifying the nuclear piRNA repertoire. Genes Dev. *29*, 1747–1762. https://doi.org/10.1101/gad.267252.115.
58. Sienski, G., Batki, J., Senti, K.A., Dönertas, D., Tirian, L., Meixner, K., and Brennecke, J. (2015). Silencio/CG9754 connects the Piwi-piRNA complex to the cellular heterochromatin machinery. Genes Dev. *29*, 2258–2271. https://doi.org/10.1101/gad.271908.115.
59. Barckmann, B., Pierson, S., Dufourt, J., Papin, C., Armenise, C., Port, F., Grentzinger, T., Chambeyron, S., Baronian, G., Desvignes, J.-P., et al. (2015). Aubergine iCLIP Reveals piRNA-Dependent Decay of mRNAs Involved in Germ Cell Development in the Early Embryo. Cell Rep. *12*, 1205–1216. https://doi.org/10.1016/j.celrep.2015.07.030.
60. Sahin, H.B., Karatas, O.F., Specchia, V., Tommaso, S.D., Diebold, C., Bozzetti, M.P., and Giangrande, A. (2016). Novel mutants of the aubergine gene. Fly (Austin) *10*, 81–90. https://doi.org/10.1080/19336934.2016.1174355.
61. Buchon, N., Broderick, N.A., Kuraishi, T., and Lemaitre, B. (2010). Drosophila EGFR pathway coordinates stem cell proliferation and gut remodeling following infection. BMC Biol. *8*, 152. https://doi.org/10.1186/1741-7007-8-152.
62. Biteau, B., and Jasper, H. (2011). EGF signaling regulates the proliferation of intestinal stem cells in Drosophila. Development *138*, 1045–1055. https://doi.org/10.1242/dev.056671.
63. Xu, N., Wang, S.Q., Tan, D., Gao, Y., Lin, G., and Xi, R. (2011). EGFR, Wingless and JAK/STAT signaling cooperatively maintain Drosophila

intestinal stem cells. Dev. Biol. *354*, 31–43. https://doi.org/10.1016/j.ydbio.2011.03.018.

64. Lin, G., Xu, N., and Xi, R. (2010). Paracrine unpaired signaling through the JAK/STAT pathway controls self-renewal and lineage differentiation of drosophila intestinal stem cells. J. Mol. Cell Biol. *2*, 37–49. https://doi.org/10.1093/jmcb/mjp028.

65. Zhou, F., Rasmussen, A., Lee, S., and Agaisse, H. (2013). The UPD3 cytokine couples environmental challenge and intestinal stem cell division through modulation of JAK/STAT signaling in the stem cell microenvironment. Dev. Biol. *373*, 383–393. https://doi.org/10.1016/j.ydbio.2012.10.023.

66. Lin, G., Xu, N., and Xi, R. (2008). Paracrine Wingless signalling controls self-renewal of Drosophila intestinal stem cells. Nature *455*, 1119–1123. https://doi.org/10.1038/nature07329.

67. Wilson, J.E., Connell, J.E., and Macdonald, P.M. (1996). aubergine enhances oskar translation in the Drosophila ovary. Development *122*, 1631–1639. https://doi.org/10.1242/dev.122.5.1631.

68. Harris, A.N., and Macdonald, P.M. (2001). aubergine encodes a Drosophila polar granule component required for pole cell formation and related to eIF2C. Development *128*, 2823–2832. https://doi.org/10.1242/dev.128.14.2823.

69. Ma, X., Zhu, X., Han, Y., Story, B., Do, T., Song, X., Wang, S., Zhang, Y., Blanchette, M., Gogol, M., et al. (2017). Aubergine Controls Germline Stem Cell Self-Renewal and Progeny Differentiation via Distinct Mechanisms. Dev. Cell *41*, 157–169.e5. https://doi.org/10.1016/j.devcel.2017.03.023.

70. Ramat, A., Garcia-Silva, M.-R., Jahan, C., Naït-Saïdi, R., Dufourt, J., Garret, C., Chartier, A., Cremaschi, J., Patel, V., Decourcelle, M., et al. (2020). The PIWI protein Aubergine recruits eIF3 to activate translation in the germ plasm. Cell Res. *30*, 421–435. https://doi.org/10.1038/s41422-020-0294-9.

71. Bonfini, A., Dobson, A.J., Duneau, D., Revah, J., Liu, X., Houtz, P., and Buchon, N. (2021). Multiscale analysis reveals that diet-dependent midgut plasticity emerges from alterations in both stem cell niche coupling and enterocyte size. eLife *10*, e64125. https://doi.org/10.7554/eLife.64125.

72. David, A., Dolan, B.P., Hickman, H.D., Knowlton, J.J., Clavarino, G., Pierre, P., Bennink, J.R., and Yewdell, J.W. (2012). Nuclear translation visualized by ribosome-bound nascent chain puromycylation. J. Cell Biol. *197*, 45–57. https://doi.org/10.1083/jcb.201112145.

73. Deliu, L.P., Ghosh, A., and Grewal, S.S. (2017). Investigation of protein synthesis in Drosophila larvae using puromycin labelling. Biol. Open *6*, 1229–1234. https://doi.org/10.1242/bio.026294.

74. Meng, F.W., and Biteau, B. (2015). A Sox Transcription Factor Is a Critical Regulator of Adult Stem Cell Proliferation in the Drosophila Intestine. Cell Rep. *13*, 906–914. https://doi.org/10.1016/j.celrep.2015.09.061.

75. Rodriguez-Fernandez, I.A., Qi, Y., and Jasper, H. (2019). Loss of a proteostatic checkpoint in intestinal stem cells contributes to age-related epithelial dysfunction. Nat. Commun. *10*, 1050. https://doi.org/10.1038/s41467-019-08982-9.

76. Pomatto, L.C.D., Sisliyan, C., Wong, S., Cline, M., Tower, J., and Davies, K.J.A. (2020). The proteasome beta 5 subunit is essential for sexually divergent adaptive homeostatic responses to oxidative stress in D. melanogaster. Free Radic. Biol. Med. *160*, 67–77. https://doi.org/10.1016/j.freeradbiomed.2020.07.003.

77. Rode, S., Ohm, H., Anhäuser, L., Wagner, M., Rosing, M., Deng, X., Sin, O., Leidel, S.A., Storkebaum, E., Rentmeister, A., et al. (2018). Differential Requirement for Translation Initiation Factor Pathways during Ecdysone-Dependent Neuronal Remodeling in Drosophila. Cell Rep. *24*, 2287–2299.e2284. https://doi.org/10.1016/j.celrep.2018.07.074.

78. Wang, R., Roiuk, M., Storer, F., Teleman, A.A., and Amoyel, M. (2025). Signals from the niche promote distinct modes of translation initiation to control stem cell differentiation and renewal in the Drosophila testis. PLoS Biol. *23*, e3003049. https://doi.org/10.1371/journal.pbio.3003049.

79. He, T.C., Sparks, A.B., Rago, C., Hermeking, H., Zawel, L., da Costa, L.T., Morin, P.J., Vogelstein, B., and Kinzler, K.W. (1998). Identification of c-MYC as a target of the APC pathway. Science *281*, 1509–1512. https://doi.org/10.1126/science.281.5382.1509.

80. Cordero, J.B., Stefanatos, R.K., Myant, K., Vidal, M., and Sansom, O.J. (2012). Non-autonomous crosstalk between the Jak/Stat and Egfr pathways mediates Apc1-driven intestinal stem cell hyperplasia in the Drosophila adult midgut. Development *139*, 4524–4535. https://doi.org/10.1242/dev.078261.

81. Qiao, D., Zeeman, A.M., Deng, W., Looijenga, L.H.J., and Lin, H. (2002). Molecular characterization of hiwi, a human member of the piwi gene family whose overexpression is correlated to seminomas. Oncogene *21*, 3988–3999. https://doi.org/10.1038/sj.onc.1205505.

82. Shi, S., Yang, Z.-Z., Liu, S., Yang, F., and Lin, H. (2020). PIWIL1 promotes gastric cancer via a piRNA-independent mechanism. Proc. Natl. Acad. Sci. USA *117*, 22390–22401. https://doi.org/10.1073/pnas.2008724117.

83. Wang, N., Tan, H.-Y., Lu, Y., Chan, Y.-T., Wang, D., Guo, W., Xu, Y., Zhang, C., Chen, F., Tang, G., and Feng, Y. (2021). PIWIL1 governs the crosstalk of cancer cell metabolism and immunosuppressive microenvironment in hepatocellular carcinoma. Signal Transduct. Target. Ther. *6*, 86. https://doi.org/10.1038/s41392-021-00485-8.

84. Huang, H., Yu, X., Han, X., Hao, J., Zhao, J., Bebek, G., Bao, S., Prayson, R.A., Khalil, A.M., Jankowsky, E., and Yu, J.S. (2021). Piwil1 Regulates Glioma Stem Cell Maintenance and Glioblastoma Progression. Cell Rep. *34*, 108522. https://doi.org/10.1016/j.celrep.2020.108522.

85. Wang, Z., Liu, N., Shi, S., Liu, S., and Lin, H. (2016). The Role of PIWIL4, an Argonaute Family Protein. J. Biol. Chem. *291*, 10646–10658. https://doi.org/10.1074/jbc.M116.723239.

86. Li, W., Martinez-Useros, J., Garcia-Carbonero, N., Fernandez-Aceñero, M.J., Ortega-Medina, L., Garcia-Botella, S., Perez-Aguirre, E., Diez-Valladares, L., and Garcia-Foncillas, J. (2019). The Prognosis Value of PIWIL1 and PIWIL2 Expression in Pancreatic Cancer. J. Clin. Med. *8*, 1275. https://doi.org/10.3390/jcm8091275.

87. Martinez, V.D., Vucic, E.A., Thu, K.L., Hubaux, R., Enfield, K.S.S., Pikor, L.A., Becker-Santos, D.D., Brown, C.J., Lam, S., and Lam, W.L. (2015). Unique somatic and malignant expression patterns implicate PIWI-interacting RNAs in cancer-type specific biology. Sci. Rep. *5*, 10423. https://doi.org/10.1038/srep10423.

88. Lin, Y., Zheng, J., and Lin, D. (2021). PIWI-interacting RNAs in human cancer. Semin. Cancer Biol. *75*, 15–28. https://doi.org/10.1016/j.semcancer.2020.08.012.

89. Krishnan, P., Ghosh, S., Graham, K., Mackey, J.R., Kovalchuk, O., and Damaraju, S. (2016). Piwi-interacting RNAs and PIWI genes as novel prognostic markers for breast cancer. Oncotarget *7*, 37944–37956.

90. Xie, K., Zhang, K., Kong, J., Wang, C., Gu, Y., Liang, C., Jiang, T., Qin, N., Liu, J., Guo, X., et al. (2018). Cancer-testis gene PIWIL1 promotes cell proliferation, migration, and invasion in lung adenocarcinoma. Cancer Med. *7*, 157–166. https://doi.org/10.1002/cam4.1248.

91. Martinez, V.D., Enfield, K.S.S., Rowbotham, D.A., and Lam, W.L. (2016). An atlas of gastric PIWI-interacting RNA transcriptomes and their utility for identifying signatures of gastric cancer recurrence. Gastric Cancer *19*, 660–665. https://doi.org/10.1007/s10120-015-0487-y.

92. Sellitto, A., Geles, K., D'Agostino, Y., Conte, M., Alexandrova, E., Rocco, D., Nassa, G., Giurato, G., Tarallo, R., Weisz, A., and Rizzo, F. (2019). Molecular and Functional Characterization of the Somatic PIWIL1/piRNA Pathway in Colorectal Cancer Cells. Cells *8*, 1390.

93. Wang, H.-L., Chen, B.-B., Cao, X.-G., Wang, J., Hu, X.-F., Mu, X.-Q., and Chen, X.-B. (2015). The clinical significances of the abnormal expressions of Piwil1 and Piwil2 in colonic adenoma and adenocarcinoma. OncoTargets Ther. *8*, 1259–1264. https://doi.org/10.2147/OTT.S77003.

94. Sun, R., Gao, C.-l., Li, D.-h., Li, B.-j., and Ding, Y.-h. (2017). Expression Status of PIWIL1 as a Prognostic Marker of Colorectal Cancer. Dis. Markers *2017*, 1204937. https://doi.org/10.1155/2017/1204937.

95. Zhou, S., Yu, L., Zhao, J., Xiao, Q., Sun, J., Wang, L., Zhou, Y., Lu, Y., Dunlop, M.G., Theodoratou, E., et al. (2025). Integration of multi-omics data to unveil the molecular landscape and role of piRNAs in early-onset colorectal cancer. BMC Med. *23*, 250. https://doi.org/10.1186/s12916-025-04074-2.

96. Araújo, T., Khayat, A., Quintana, L., Calcagno, D., Mourão, R., Modesto, A., Paiva, J., Lima, A., Moreira, F., Oliveira, E., et al. (2018). Piwi like RNA-mediated gene silencing 1 gene as a possible major player in gastric cancer. World J. Gastroenterol. *24*, 5338–5350. https://doi.org/10.3748/wjg.v24.i47.5338.

97. Guinney, J., Dienstmann, R., Wang, X., de Reyniès, A., Schlicker, A., Soneson, C., Marisa, L., Roepman, P., Nyamundanda, G., Angelino, P., et al. (2015). The consensus molecular subtypes of colorectal cancer. Nat. Med. *21*, 1350–1356. https://doi.org/10.1038/nm.3967.

98. Sansom, O.J., Meniel, V.S., Muncan, V., Phesse, T.J., Wilkins, J.A., Reed, K.R., Vass, J.K., Athineos, D., Clevers, H., and Clarke, A.R. (2007). Myc deletion rescues Apc deficiency in the small intestine. Nature *446*, 676–679. https://doi.org/10.1038/nature05674.

99. Rennoll, S., and Yochum, G. (2015). Regulation of MYC gene expression by aberrant Wnt/β-catenin signaling in colorectal cancer. World J. Biol. Chem. *6*, 290–300. https://doi.org/10.4331/wjbc.v6.i4.290.

100. Lee, W.C., Beebe, K., Sudmeier, L., and Micchelli, C.A. (2009). Adenomatous polyposis coli regulates Drosophila intestinal stem cell proliferation. Development *136*, 2255–2264. https://doi.org/10.1242/dev.035196.

101. Dufourt, J., Bontonou, G., Chartier, A., Jahan, C., Meunier, A.-C., Pierson, S., Harrison, P.F., Papin, C., Beilharz, T.H., and Simonelig, M. (2017). piRNAs and Aubergine cooperate with Wispy poly(A) polymerase to stabilize mRNAs in the germ plasm. Nat. Commun. *8*, 1305. https://doi.org/10.1038/s41467-017-01431-5.

102. Becalska, A.N., Kim, Y.R., Belletier, N.G., Lerit, D.A., Sinsimer, K.S., and Gavis, E.R. (2011). Aubergine is a component of a nanos mRNA localization complex. Dev. Biol. *349*, 46–52. https://doi.org/10.1016/j.ydbio.2010.10.002.

103. Cook, H.A., Koppetsch, B.S., Wu, J., and Theurkauf, W.E. (2004). The Drosophila SDE3 Homolog armitage Is Required for oskar mRNA Silencing and Embryonic Axis Specification. Cell *116*, 817–829. https://doi.org/10.1016/S0092-8674(04)00250-8.

104. Movafagh, S., Crook, S., and Vo, K. (2015). Regulation of hypoxia-inducible factor-1a by reactive oxygen species: new developments in an old debate. J. Cell. Biochem. *116*, 696–703. https://doi.org/10.1002/jcb.25074.

105. Hinnebusch, A.G. (2014). The Scanning Mechanism of Eukaryotic Translation Initiation. Annu. Rev. Biochem. *83*, 779–812. https://doi.org/10.1146/annurev-biochem-060713-035802.

106. Lee, A.S., Kranzusch, P.J., Doudna, J.A., and Cate, J.H.D. (2016). eIF3d is an mRNA cap-binding protein that is required for specialized translation initiation. Nature *536*, 96–99. https://doi.org/10.1038/nature18954.

107. Roiuk, M., Neff, M., and Teleman, A.A. (2024). eIF4E-independent translation is largely eIF3d-dependent. Nat. Commun. *15*, 6692. https://doi.org/10.1038/s41467-024-51027-z.

108. Lee, A.S.Y., Kranzusch, P.J., and Cate, J.H.D. (2015). eIF3 targets cell-proliferation messenger RNAs for translational activation or repression. Nature *522*, 111–114. https://doi.org/10.1038/nature14267.

109. Song, P., Yang, F., Jin, H., and Wang, X. (2021). The regulation of protein translation and its implications for cancer. Signal Transduct. Target. Ther. *6*, 68. https://doi.org/10.1038/s41392-020-00444-9.

110. Schatoff, E.M., Leach, B.I., and Dow, L.E. (2017). WNT Signaling and Colorectal Cancer. Curr. Colorectal Cancer Rep. *13*, 101–110. https://doi.org/10.1007/s11888-017-0354-9.

111. Wiegering, A., Uthe, F.W., Jamieson, T., Ruoss, Y., Hüttenrauch, M., Küspert, M., Pfann, C., Nixon, C., Herold, S., Walz, S., et al. (2015). Targeting Translation Initiation Bypasses Signaling Crosstalk Mechanisms That Maintain High MYC Levels in Colorectal Cancer. Cancer Discov. *5*, 768–781. https://doi.org/10.1158/2159-8290.Cd-14-1040.

112. Knight, J.R.P., Alexandrou, C., Skalka, G.L., Vlahov, N., Pennel, K., Officer, L., Teodosio, A., Kanellos, G., Gay, D.M., May-Wilson, S., et al. (2021). MNK Inhibition Sensitizes KRAS-Mutant Colorectal Cancer to mTORC1 Inhibition by Reducing eIF4E Phosphorylation and c-MYC Expression. Cancer Discov. *11*, 1228–1247. https://doi.org/10.1158/2159-8290.Cd-20-0652.

113. Waldron, J.A., Kanellos, G., Smith, R.C.L., Knight, J.R.P., Munro, J., Alexandrou, C., Vlahov, N., Pardo-Fernandez, L., Moore, M., Gillen, S.L., et al. (2023). eIF4A1 is essential for reprogramming the translational landscape of Wnt-driven colorectal cancers. bioRxiv. https://doi.org/10.1101/2023.11.10.566546.

114. Goh, S.H., Hong, S.H., Hong, S.H., Lee, B.C., Ju, M.H., Jeong, J.S., Cho, Y.R., Kim, I.H., and Lee, Y.S. (2011). eIF3m expression influences the regulation of tumorigenesis-related genes in human colon cancer. Oncogene *30*, 398–409. https://doi.org/10.1038/onc.2010.422.

115. Vourekas, A., Alexiou, P., Vrettos, N., Maragkakis, M., and Mourelatos, Z. (2016). Sequence-dependent but not sequence-specific piRNA adhesion traps mRNAs to the germ plasm. Nature *531*, 390–394. https://doi.org/10.1038/nature17150.

116. Gainetdinov, I., Vega-Badillo, J., Cecchini, K., Bagci, A., Colpan, C., De, D., Bailey, S., Arif, A., Wu, P.H., MacRae, I.J., and Zamore, P.D. (2023). Relaxed targeting rules help PIWI proteins silence transposons. Nature *619*, 394–402. https://doi.org/10.1038/s41586-023-06257-4.

117. Li, F., Yuan, P., Rao, M., Jin, C.-H., Tang, W., Rong, Y.-F., Hu, Y.-P., Zhang, F., Wei, T., Yin, Q., et al. (2020). piRNA-independent function of PIWIL1 as a co-activator for anaphase promoting complex/cyclosome to drive pancreatic cancer metastasis. Nat. Cell Biol. *22*, 425–438. https://doi.org/10.1038/s41556-020-0486-z.

118. Luhur, A., Mariyappa, D., Bohall, P., Multini, L., Elkins, M., and Zelhof, A.C. (2025). Establishment of Drosophila intestinal cell lines as tools for multiomic screening and deciphering intestinal biology. Sci. Rep. *15*, 32291. https://doi.org/10.1038/s41598-025-17336-z.

119. Lomaev, D., Mikhailova, A., Erokhin, M., Shaposhnikov, A.V., Moresco, J.J., Blokhina, T., Wolle, D., Aoki, T., Ryabykh, V., Yates, J.R., 3rd., et al. (2017). The GAGA factor regulatory network: Identification of GAGA factor associated proteins. PLoS One *12*, e0173602. https://doi.org/10.1371/journal.pone.0173602.

120. Ghosh, S., and Lasko, P. (2015). Loss-of-function analysis reveals distinct requirements of the translation initiation factors eIF4E, eIF4E-3, eIF4G and eIF4G2 in Drosophila spermatogenesis. PLoS One *10*, e0122519. https://doi.org/10.1371/journal.pone.0122519.

121. Schindelin, J., Arganda-Carreras, I., Frise, E., Kaynig, V., Longair, M., Pietzsch, T., Preibisch, S., Rueden, C., Saalfeld, S., Schmid, B., et al. (2012). Fiji: an open-source platform for biological-image analysis. Nat. Methods *9*, 676–682. https://doi.org/10.1038/nmeth.2019.

122. Mi, H., Muruganujan, A., Huang, X., Ebert, D., Mills, C., Guo, X., and Thomas, P.D. (2019). Protocol Update for large-scale genome and gene function analysis with the PANTHER classification system (v.14.0). Nat. Protoc. *14*, 703–721. https://doi.org/10.1038/s41596-019-0128-8.

123. Marshall, O.J. (2004). PerlPrimer: cross-platform, graphical primer design for standard, bisulphite and real-time PCR. Bioinformatics *20*, 2471–2472. https://doi.org/10.1093/bioinformatics/bth254.

124. Bischof, J., Maeda, R.K., Hediger, M., Karch, F., and Basler, K. (2007). An optimized transgenesis system for Drosophila using germ-line-specific phiC31 integrases. Proc. Natl. Acad. Sci. USA *104*, 3312–3317. https://doi.org/10.1073/pnas.0611511104.

125. Hafner, M., Landgraf, P., Ludwig, J., Rice, A., Ojo, T., Lin, C., Holoch, D., Lim, C., and Tuschl, T. (2008). Identification of microRNAs and other small regulatory RNAs using cDNA library sequencing. Methods *44*, 3–12. https://doi.org/10.1016/j.ymeth.2007.09.009.

126. Akbergenov, R., Si-Ammour, A., Blevins, T., Amin, I., Kutter, C., Vanderschuren, H., Zhang, P., Gruissem, W., Meins, F., Jr., Hohn, T., and Poogin, M.M. (2006). Molecular characterization of geminivirus-derived small RNAs in different plant species. Nucleic Acids Res. *34*, 462–471. https://doi.org/10.1093/nar/gkj447.

127. Trejo, C.L., Babić, M., Imler, E., Gonzalez, M., Bibikov, S.I., Shepard, P.J., VanSteenhouse, H.C., Yeakley, J.M., and Seligmann, B.E. (2019). Extraction-free whole transcriptome gene expression analysis of FFPE sections and histology-directed subareas of tissue. PLoS One *14*, e0212031. https://doi.org/10.1371/journal.pone.0212031.

STAR★METHODS

KEY RESOURCES TABLE

REAGENT or RESOURCE	SOURCE	IDENTIFIER
Antibodies		
Rabbit anti-Aubergine (1:100)	Phillipe Zamore; UMass Medical School, USA[6]	N/A
Mouse anti-Armadillo, 1:3	Developmental Studies Hybridoma Bank	Cat# N2 7A1; RRID: AB_528089
Chicken anti-GFP, 1:4000	Abcam	Cat# ab13970; RRID: AB_300798
Rabbit anti-eIF3C, 1:100	Yulii Shidlovskii; Institute of Gene Biology, Russia.[119]	N/A
Rabbit anti-eIF4G, 1:100	Paul Lasko, McGill University, Canada.[120]	N/A
Rabbit anti-pH3 S10, 1:100	Cell Signaling	Cat# 9701; RRID: AB_331535
Mouse anti-Multiubiquitin chain (Clone FK1), 1:100	Cayman Chemical	Cat# Cay14219-100
Guinea pig anti-Myc 1:100	Ginés Morata; CSIC-Madrid	N/A
Rabbit anti-Piwil1 1:200	Abcam	Abcam Cat# ab12337, RRID:AB_470241
Mouse anti-Puromycin 1:100	Developmental Studies Hybridoma Bank	DSHB Cat# PMY-2A4; RRID:AB_2619605
Rabbit anti-Sox21a 1:2000	Benoît Biteau; University of Rochester-NY, USA	N/A
Mouse anti-Wingless 1:10	Developmental Studies Hybridoma Bank	DSHB Cat# 4d4; RRID:AB_528512
Goat Alexa Fluor anti-chicken IgY 488, 1:100	Invitrogen	Cat# A-11039; RRID: AB_142924
Goat Alexa Fluor anti-mouse IgG 647, 1:100	Invitrogen	Cat# A-21235; RRID: AB_2535804
Goat Alexa Fluor anti-Rabbit IgG 488, 1:100	Invitrogen	Cat# A-11008; RRID: AB_143165
Goat Alexa Fluor anti-Rabbit IgG 594, 1:100	Invitrogen	Cat# A-11072, RRID: AB_142057
Goat Alexa Fluor anti-mouse IgG 594, 1:100	Invitrogen	Cat# A-11032; RRID: AB_2534091
Bacterial and virus strains		
Pseudomonas entomophila	Bruno Lemaitre; EPFL-Lausanne	N/A
Stbl3 chemically competent E. coli	Invitrogen	C737303
pCMV-VSV-G	Addgene	N/A
psPAX2	Addgene	N/A
TRC Lentiviral shRNA for human PIWIL1	Horizon discovery	TRCN0000007876; TRCN0000007877; TRCN0000007878; TRCN0000007879; TRCN0000007880
TRC Lentiviral Non-targeting control shRNA	Horizon discovery	RHS6848
Biological samples		
Human Intestinal Polyp-derived organoids	IGC, University of Edinburgh, UK	MD22750-Polyp1 and Polyp 4; MD23182-Polyp 1
Grade 4 intestinal cancer-derived organoids	IGC, University of Edinburgh, UK	MD20043T; MD23182T
Metastatic human intestinal cancer-derived organoid	IGC, University of Edinburgh, UK	MD23169T
Intestinal cancer liver metastasis tissue	IGC, University of Edinburgh, UK	MD23169-LIVMET
Human Colorectal Cancer Tissue Microarray	Greater Glasgow and Clyde NHS Biorepository and Glasgow Tissue Research Facility under ethical approval number: 16/WS/0207	Glasgow Safehaven GSH/18/ON007
Chemicals, peptides, and recombinant proteins		
A83-01	Tocris	Cat# 2939
Advanced DMEM/F12 (ADF) media	Invitrogen	Cat# 12634-028

(*Continued on next page*)

Continued

REAGENT or RESOURCE	SOURCE	IDENTIFIER
B27	Invitrogen	Cat# 12587-010
BME-2 phenol red	Biotechne	Cat# 3533-010-02P
Bond Diluent	Leica	AR9352
Bond Wash prior to primary antibody application	Leica	AR9590
Bovine Serum Albumin	Sigma-Aldrich	Cat# A3294
CellTrics 30μm filters	Sysmex	Cat# 04-0042-2316
Countless Cell Counting Chamber Slides	Life Technologies	Cat# C10228
DAPI	Sigma-Aldrich	Cat# D9542
Dewax Solution	Leica	AR9222
Dimethyl Sulfoxide	Thermo Fisher Scientific	Cat# 10500151
DNAse	Thermo Fisher Scientific	Cat# 18068015
DPX	CellPath	SEA-1300-00A
EGF	Peprotech	Cat# AF-100-15
Elastase from porcine pancreas	Sigma-Aldrich	Cat# E0258
Epitope Retrieval solution 2 (ER2)	Leica	AR9640
Gastrin	Sigma-Aldrich	Cat# G9145
1M HEPES	Life Technologies	Cat# 15630-056
Hexadimethrine bromide (Polybrene)	Sigma-Aldrich	Cat# H9268-5G
High-Capacity cDNA Reverse Transcription Kit	Thermo Fisher Scientific	Cat# 4368813
Intense R Kit	Leica	DS9263
IntestiCult Organoid Growth Medium (Human)	Stem Cell Technologies	Cat# 06010
Methanol	Fisher Scientific	Cat# 10675112
N-Acetyl-L-cysteine (NAC treatment for flies)	Sigma-Aldrich	Cat# A7250
N-Acetyl-L-cysteine (organoids culture)	Sigma-Aldrich	Cat# A9165
Neutral Buffered Formalin	Solmedia	FORM5000
Nicotinamide	Sigma-Aldrich	Car# N0636
Noggin conditioned media	Labmade Myant's lab	N/A
P38i (SB202190)	Sigma-Aldrich	Cat# S7067
Paraformaldehyde	Polysciences Inc	Cat#18814-20
PerfeCTa SYBR Green FastMix Low ROX 1250 Reactions (experiments in *Drosophila*)	Quantabio	Cat# 95074-012
PGE2	Tocris	Cat# 2296
Primocin	Invivogen	Cat# ANT-PM1
Puromycin (organoids selection)	Gibco	Cat#A11138-03
Puromycin (Translation assay)	Sigma-Aldrich	Cat# P8833
qScript cDNA SuperMix	VWR	Cat# 95048-100
Resazurin	Bio-Techne	Cat# AR002
RNAscope 2.5 LS Reagent Kit-Brown	ACD	Cat# 322100
RNase-Free DNase set	Qiagen	Cat# 79254
RNaseZap RNase Decontamination Solution	Invitrogen	Cat# 9780
RNeasy Mini Kit	Qiagen	Cat# 74104/Cat# 74106
Schneider's Insect Medium	Sigma-Aldrich	Cat# S0146
Sucrose	Fisher Scientific	Cat# 10634932
Sybr green (experiments in organoids)	Life Technologies	Cat#4472920
Triton X-100	Sigma-Aldrich	Cat# X100

(*Continued on next page*)

Continued

REAGENT or RESOURCE	SOURCE	IDENTIFIER
TRIzol Reagent	Thermo Fisher Scientific	Cat# 15596026
TrypIE Express Phenol Red	Life Technologies	Cat# 12605010
Valproic Acid (VPA)	Sigma-Aldrich	Cat# PHR1061-1G
VECTASHIELD Antifade Mounting Medium with DAPI	Vector Laboratories	Cat# H-1200
Wash buffer prior to secondary antibody application	Agilent	K4003
Whatman GF/B Glass microfiber filters Diameter 21mm	Whatman	Cat# 1821021
Y27632	Tocris	Cat# 1254/10
KAPA Long Range DNA polymerase	Sigma-Aldrich	Cat# KK3502
NEB Next Ultra Directional II RNA Library Prep Kit for Illumina	NEB	Cat# E7760
oligo d(T)25 magnetic beads	NEB	Cat# S1419
sodium periodate	Sigma-Aldrich	Cat# 311448
Super Script II	Thermo Fisher	SuperScript II
T4 RNA Ligase 1	NEB	T4 RNA Ligase 1
T4 RNA Ligase 2, truncated KQ	NEB	T4 RNA Ligase 2, truncated KQ
Deposited data		
Small RNA sequencing	This study	GEO: GSE253621; https://www.ncbi.nlm.nih.gov/geo/query/acc.cgi?acc=GSE253621
mRNA sequencing	This study	GEO: GSE253624; https://www.ncbi.nlm.nih.gov/geo/query/acc.cgi?acc=GSE253624
General code information and information on transgenic line generation	This study	https://github.com/RippeiHayashi/gut_aubergine
New codes generated	This study	https://doi.org/10.5281/zenodo.18608988
Source data files	This study	https://doi.org/10.5525/gla.researchdata.2169
TempOSeq RNA seq data from CRC patients	N/A	NCBI: PRJNA997336
Experimental models: Cell lines		
HEK293T cells for shRNA virus production	Kevin Myant; University of Edinburgh, UK	N/A
Noggin producing cell line	Hans Clevers; Hubrecht Institute, Netherlands	N/A
Piwil1tm1Hfl/Mmmh (miwi null)	MMRRC	Backcrossed to a *C57BL6* background
Experimental models: *Drosophila melanogaster*		
w^{1118}	Ross Gagan; University of Glasgow, UK	N/A
yw; escargot-Gal4/CyO; MKRS/TM6B	Cordero Lab; University of Glasgow, UK	N/A
yw; escargot-Gal4, UAS-GFP/CyO	Cordero Lab; University of Glasgow, UK	N/A
escargot-gal4, aub[HN2] cn[1] bw[1]/CyO	This study	N/A
yw; escargot-Gal4, UAS-GFP/CyO; tub-Gal80^{ts}/TM6B	S. Hayashi; Rinken Centre-Japan	N/A
UAS-Dicer 2; escargot-Gal4, UAS-GFP; tub-Gal80^{ts}/S-T	Cordero Lab; University of Glasgow, UK	N/A
escargot-Gal4, UAS 2xEYFP/CyO; Su(H) GBE-Gal80, tub-Gal80^{ts}/TM6B	S. Hou; Fudan University, China	N/A
Su(H) GBE-Gal4, UAS CD8 GFP/CyO; tub-Gal80^{ts}/TM6B	Allison Bardin; Curie Institute, France	N/A
y, w, hsFLP/+; UAS-CD8-GFP, tub-Gal4/+; FRT82B, tubGal80/TM6B	David Bilder; Berkeley University, USA	N/A

(*Continued on next page*)

Continued

REAGENT or RESOURCE	SOURCE	IDENTIFIER
FRT82B, con LacZ/TM6B	Cordero Lab; University of Glasgow, UK	N/A
w[1118]; P{w[+mC]=GAL4::VP16-nanos.UTR}CG6325[MVD1]	Bloomington Drosophila Stock Center	#4937
aub^{HN2}/CyO; nanos-Gal4/TM6B	This study	N/A
UAS-aub^{RNAi}/CyO	Vienna Drosophila Resource Center	#106999
UAS-aubRNAi/CyO, FRT82B, con LacZ/TM6B	This study	N/A
y[1] v[1]; P{y[+t7.7] v[+t1.8]=TRiP.JF01390}attP2	Bloomington Drosophila Stock Center	#31606
y[1] sc[*] v[1] sev[21]; P{y[+t7.7] v[+t1.8]=TRiP.HMS00119}attP2	Bloomington Drosophila Stock Center	#34810
UAS-aub^{RNAi}/CyO; UAS-prosbeta5^{RNAi}/TM6B	This study	N/A
UAS-nRFP Red Stinger 6/TM6B	Benjamin White; NIH, USA	N/A
w; UAS-aub^{RNAi}/CyO; UAS-nRFP Red Stinger 6/TM6B	This study	N/A
UAS-wg::HA/TM6B	Bloomington Drosophila Stock Center	#5918
UAS-aubRNAi/CyO; UAS-wg::HA/TM6B	This study	N/A
UAS-aub^{WT}/TM6B	This study	N/A
UAS-aub^{AA}/TM6B	This study	N/A
UAS-aub^{ADH}/TM6B	This study	N/A
aub[HN2] cn[1] bw[1]/CyO	Bloomington Drosophila Stock Center	#8517
w[1118]; aub[QC42] cn[1] bw[1]/CyO, P{ry[+t7.2]=sevRas1.V12}FK1	Bloomington Drosophila Stock Center	#4968
aub^{QC42}/CyO, UAS-aub^{WT}/TM6B	This study	N/A
aub^{QC42}/CyO, UAS-aub^{AA}/TM6B	This study	N/A
aub^{QC42}/CyO, UAS-aub^{ADH}/TM6B	This study	N/A
w[1118]; P{ry[+t7.2]=PZ}piwi[1]/CyO, P{w[+mC]=ActGFP}JMR1	Bloomington Drosophila Stock Center	#43637
w[1118]; P{ry[+t7.2]=ry11}piwi[2]/CyO, P{w[+mC]=ActGFP}JMR1	Bloomington Drosophila Stock Center	#43319
bw[1]; st[1] AGO3[t2]/TM6B, Tb[1]	Bloomington Drosophila Stock Center	#28269
bw[1]; st[1] AGO3[t3]/TM6B, Tb[1]	Bloomington Drosophila Stock Center	#28270
P{ry[+t7.2]=neoFRT}82B ry[506] spn-E[hls-Delta125] e[1]/TM3, ry[*] Sb[1]	Bloomington Drosophila Stock Center	#43638
spn-E [100.37]	Vienna Drosophila Resource Center	#313105
UAS-eIF3CRNAi	Vienna Drosophila Resource Center	#26667
UAS-eIF3CRNAi	Vienna Drosophila Resource Center	#26664
UAS-eIF3GRNAi	Bloomington Drosophila Stock Center	#43243 (no longer available)
UAS-eIF3mRNAi	Bloomington Drosophila Stock Center	#32879
UAS-eIF3mRNAi	Vienna Drosophila Resource Center	#110359
UAS-mycRNAi	Vienna Drosophila Resource Center	#2947
UAS-stringRNAi	Vienna Drosophila Resource Center	#36094
w[*]; P{w[+mC]=UASp-GFP-aub.H}8.1	Bloomington Drosophila Stock Center	#42219
UAS-eIF4GRNAi	Bloomington Drosophila Stock Center	#33049
w-;; APC1q8, FRT82B/TM6B	Y.Ahmed; Geisel School of Medicine-Dartmouth, NH-USA	N/A
UAS-aub^{RNAi}/CyO, APC1q8, FRT82B/TM6B	This study	N/A

(*Continued on next page*)

Continued

REAGENT or RESOURCE	SOURCE	IDENTIFIER
Oligonucleotides		
19 mer RNA spike for small RNA library preparation: CGUACGCGGGUUUAAACGA	This study	N/A
35 mer RNA spike for small RNA library preparation: CUCAUCUUGGUCGUACG CGGAAUAGUUUAAACUGU	This study	N/A
3′ adapter for small RNA library preparation: 5rApp/NNNNAGAT CGGAAGAGCACACGTCT/3ddC	This study	N/A
5′ adapter for small RNA library preparation: ACACUCUUUCCCUACACGAC GCUCUUCCGAUCUNNNN	This study	N/A
Drosophila ago3 Forward: GCGAGACGAAGTACGGTCAGATAAC	This study	N/A
Drosophila ago3 Reverse: CAATCAAATAAGCCAATTTGTGAGCG	This study	N/A
Drosophila aub Forward: CGCTGACTTTAGGACGTTGAG	This study	N/A
Drosophila aub Reverse: GGTCTCTACACTCTGTTTACACGA	This study	N/A
Drosophila aub Forward: GGCACTTACTCCCAAGCGAT	This study	N/A
Drosophila aub Reverse: TGTCGAGHGCGCGATAACTTT	This study	N/A
Drosophila esg Forward: GCTGCAAGGATTGTGACAAGA	This study	N/A
Drosophila esg Reverse: AGATTCGAGCGATCTGCAAA	This study	N/A
Drosophila myc Forward: ATGCACATCACCGATCACAG	This study	N/A
Drosophila myc Reverse: ATGGGCCATCTGGAACTGTA	This study	N/A
Drosophila piwi Forward: TGCGCTCAAACTTTCAGCTTA	This study	N/A
Drosophila piwi Reverse: GTGGTTAAAAGCGCGCAATC	This study	N/A
Drosophila rpl32 Forward: AGGCCCAAGATCGTGAAGAA	This study	N/A
Drosophila rpl32 Reverse: TGTGCACCAGGAACTTCTTGAA	This study	N/A
Drosophila socs36E Forward: CAAGTTCAGCTTCGACTGCC	This study	N/A
Drosophila socs36E Reverse: GCTCGAAGAACATCACGCAG	This study	N/A
Drosophila sox21a Forward: AGACAATTAATACAGAGCTCGAGG	This study	N/A
Drosophila sox21a Reverse: GAGATGCTCGTCATGATGCC	This study	N/A
Human *β-actin* Forward: CATGTACGTTGCTATCCAGGC	This study	N/A

(*Continued on next page*)

Continued

REAGENT or RESOURCE	SOURCE	IDENTIFIER
Human *β-actin* Reverse: CTCCTTAATGTCACGCACGAT	This study	N/A
Human *LGR5* Forward: TCAGGAGTTATCGTTAGCAGAGA	This study	N/A
Human *LGR5* Reverse: TGTCAGCCGGAAATGGTTAGT	This study	N/A
Human *PIWIL1* Forward: GGCTCCTGGCAAAAGGTCA	This study	N/A
Human *PIWIL1* Reverse: GAGGTCTAGGTAGGAGGTGAAG	This study	N/A
Recombinant RNA		
ShPIWIL1-1	Horizon Discovery	Cat# RHS3979-201740149
ShPIWIL1-2	Horizon Discovery	Cat# RHS3979-201740151
Software and algorithms		
Adobe Illustrator 2025	Adobe	
BioRender	BioRender	License Agreement: UZ28NVH244
Fiji	N/A	NIH;Schindelin et al.[121]
HALO System	Indica labs	N/A
GraphPad Prism 6	GraphPad	N/A
PANTHER 17.0 Classification System	N/A	Mi et al.[122]
PerlPrimer	N/A	Marshall[123]
R and R studio	CRAN	N/A
SPSS version 8	IBM	N/A
Zen 2.0 (blue edition)	Zeiss	N/A
Zen 3.0	Zeiss	N/A
7500 Real-Time PCR Software	Applied Biosystems	N/A
Other		
Axio Observer microscope	Zeiss	N/A
BX51 microscope	Olympus	N/A
FACSAria Fusion Flow Cytometer	BD Biosciences	N/A
LSM710 Confocal Microscope	Zeiss	N/A
LSM780 Confocal Microscope	Zeiss	N/A

EXPERIMENTAL MODEL AND STUDY PARTICIPANT DETAILS

Drosophila melanogaster stocks rearing, maintenance, and timelines of genetic manipulations

A complete list of fly strains used in this paper is included in the key resources table. Full genotypes for fly lines used in each figure are described in Table S1. Fly stocks were kept in temperature and humidity-controlled incubators set up with a 12h–12h light/dark cycle. For experiments with *aub* mutant lines, crosses were performed at 25°C and the desired F1 progeny was sorted 2/3 days after adult eclosion and kept at 25°C for 5–7 days before dissection. For experiments using the *GAL4/GAL80*^{ts} system, flies were crossed at 18°C. The desired F1 progeny was sorted 2/3 days after adult eclosion and was kept at 18°C for 5 days before being transferred to 29°C to allow transgenes activation. In most cases, transgene expression was done for 5–8 days prior to functional experiments. However, in *Aub* gain of function experiments, transgenes were overexpressed for 10 days. Crosses were performed at 25°C and parental lines were flipped twice a week. For MARCM clones, adults of the desired genotype were aged for 3 to 5 days at 25°C before undergoing three 30 min heat shocks in one day, in a 37°C water bath. Heat shocked adults were then aged for 7days, 10 days or 14 days at 25°C before dissection. In all cases, experimental flies were flipped every two days on fresh food. Only mated females were used for experiments.

Human patient information and ethics statement

The human cohort analyzed contains 1030 colorectal cancer patients who had undergone elective and potentially curative resection of stage I-III colorectal adenocarcinoma in a single surgical unit at the Glasgow Royal Infirmary, Western Infirmary or Stobhill Hospitals (Glasgow, UK) between 1997 and 2007. Resection was considered curative based on pre-operative computed tomography

and intra-operative findings. The data are stored within the Glasgow Safehaven (GSH21ON009) and ethical approval was in place for the study (MREC/01/0/36).

Human patient-derived organoids (PDOs)

The human derived PDOs used in this study were generated in the Edinburgh component of the CRUK Scotland Center under the supervision and direction of MGD and FVND, University of Edinburgh: MD20043 is an 81-year-old male with Stage 4 rectal cancer, (T3N2M1). MD23169 is male with Stage 4 ascending colon tumor along with current liver metastasis (T3N1M1). Ethical approval for human CRC organoid derivation was carried out under NHS Lothian Ethical Approval Scottish Colorectal Cancer Genetic Susceptibility Study 3 (SOCCS3) (REC ref. 11/SS/0109). All patients provided fully informed consent for analysis of tumor and normal tissue that was surplus to requirements for pathological assessment, clinical annotation and generation of organoids.

METHOD DETAILS

Human organoid culture media and shPIWIL1 knockdown

Human carcinoma organoids were cultured in PDO media containing 1% Noggin conditioned media, 1x B27, 50 ng/mL EGF, 10 nM Gastrin, 10 nM PGE2, 10 mM Nicotinamide, 10 μM SB202190, 600 nM A83-01, 12.5 mM N-Acetylcysteine in ADF (with 1X PenStrep, HEPES, Glutamine, 100 μg/mL Primocin).

For transduction conditions, human organoids were pre-treated with IntestiCult organoid growth media (OGM) and VPA (1:10,000) for 48h after 2 days post-split (Day −1). On transduction day (Day1), human organoids were digested into single-cell suspension in TrypLE with 10 μM Y27632 for 8 min at 37°C with mechanical dissociation every 4 min. Single cell suspension (with 8 μg/mL Polybrene) were combined with viral particles containing, TRC non-targeting (NT) control, TRC shPIWIL1-1 (76), and shPIWIL1-2 (78) and placed on BME layer. On Day2, media was changed into IntestiCult OGM + VPA (1:10,000) + 10 μM Y27632. On Day3, antibiotic selection started with 2 μg/mL Puromycin in IntestiCult OGM. On Day6, RNA and protein samples are collected, and colony formation ability (clonogenicity) assay started. For clonogenicity, organoids from Day 6 were collected, washed once or twice with ice-cold PBS. Then, human organoids were digested into single-cell suspension in TrypLE with 10 μM Y27632 for 5–8 min at 37°C with mechanical dissociation every 3–4 min. 2000 single cells in 5 μL BME drops per well were plated and IntestiCult OGM with 2 μg/mL Puromycin added after 15 min to set BME. Organoid formation was observed throughout the clonogenicity assay. On Day 14, organoid numbers were counted manually on Leica Light microscope and pictures were taken on EVOS FL Cell Imaging System. For cell viability, the media was replaced with fresh media containing 10% Resazurin for 24h in 37°C incubator. The next day, relative cell viability was measured with a TECAN Spark microplate reader in 96-well plate with three technical replicates. IntestiCult OGM media was used exclusively during transduction and the single-cell stage of organoid development for clonogenicity assays. Otherwise, only PDO media was utilized for maintaining the organoids.

Damage-induced intestinal regeneration

To induce intestinal regeneration, mated female flies were fed on filters (Whatman) soaked in 5% sucrose only (control condition) or with the pathogenic bacteria *Pseudomonas entomophila* (*Pe*) at OD_{600} = 25 (damage condition) for 16 h prior to dissection. The bacterial solution was obtained after overnight culture in LB medium at 29°C under 220 rpm shaking overnight, after which bacteria were pelleted (Beckman Coulter JS-4.2 rotor, 10 min, 4000 rpm) and diluted in a solution of 5% sucrose to reach OD_{600} = 25.

Immunohistochemistry

Drosophila tissue

The dissection of guts was performed in PBS at room temperature and 16 h after feeding the mated female flies with sucrose or *Pe*. After dissection, guts were immediately fixed in solution of 4% paraformaldehyde (Polysciences Inc) for 1 h. Tissues were then washed in PBST (PBS with Triton 0.2%) before incubation overnight at 4°C with the primary antibodies diluted in blocking solution PBT (with 0.5% BSA). The day after, guts were washed 3 × 15 min with PBST at room temperature before incubation with the secondary antibodies for 2 h at room temperature. Guts were then washed 3 × 15 min with PBST at room temperature before mounting in DAPI containing mounting media. Slides were kept at 4°C before imaging. To improve Arm and Aub staining, guts were placed in methanol for 10 min at room temperature after the fixation step with 4% paraformaldehyde.

Human and mouse tissue

Immunohistochemistry (IHC) staining was performed on a previously constructed human tissue microarray or on 4 μm formalin fixed paraffin embedded sections, which had previously been incubated in a 60°C oven for 2 h. Tissue slides for PIWIL1 detection were stained on a Leica Bond Rx Automated Stainer. Samples underwent on-board dewaxing and epitope retrieval using ER2 solution (Leica) for 20 min at 95°C. Sections were rinsed with Leica wash buffer before peroxidase block was performed using an Intense R kit (Leica) for 5 min. Sections were rinsed with wash buffer (Leica) before anti-PIWIL1 application at an optimal dilution (1/200). The sections were then rinsed with wash buffer (Agilent) for 30 min, before secondary antibody application. The sections were rinsed with wash buffer, visualized using DAB and counterstained with Haematoxylin in the Intense R kit. To complete the IHC staining sections were rinsed in tap water, dehydrated through a series of graded alcohols, and placed in xylene. The stained sections were cover slipped in xylene using DPX mounting.

NAC treatment

Flies were placed in empty vials with filters soaked with a 5% sucrose solution alone or containing 20 mM NAC 48h prior dissection. Flies were then fed with either sucrose; *Pe* (OD_{600} = 25); 5% sucrose + 20 mM NAC or 5% sucrose + 20 mM NAC + *Pe* (OD_{600} = 25) 16h prior dissection.

Generation of *aub* transgenes

The three pUASt-attB-GFP constructs of *aub* were generated for this study. A complementary DNA (cDNA) of *aub* was amplified from w^{1118} flies and cloned into the pUASt-attB plasmid, that was originally made by the Basler group (GenBank accession EF362409)[124] and received as a gift from Julius Brennecke. A GFP cDNA was inserted N-terminally to *aub* cDNA. Standard site-directed mutagenesis was used to introduce amino acid substitutions to generate aub^{AA} (Y345A/Y346A,[59]) and aub^{ADH} (D636A,[19]). Plasmid construction and sequences are available at https://github.com/RippeiHayashi/gut_aubergine.

Egg laying/eclosion assay

Crosses to obtain experimental animals were kept at 18°C. Virgin females of the desired genotype were selected and placed into fresh vials and allowed to mate with w^{1118} males. A maximum of 5 females and 5 males were housed in each vial and allowed to mate over a period of 24 h at 18°C. The following day, males were removed, and females were moved onto fresh food and incubated at 25°C. Females were flipped into new vials every 24 h. The number of eggs in each vial was counted and recorded at the same time. This process was repeated 3 more times. Importantly, the number of live females was recorded each time, at the time of flipping. Any females that died during the night were included in the eggs/adult ratio but were excluded from the subsequent recordings. Three replicates of these experiments were performed.

Protein translation assay

For general protein translation assessment, flies were fed on filters (Whatman) soaked in 5% sucrose only or with *Pe* OD_{600} = 25 16 h prior to gut dissection in Schneider's insect medium (Sigma-Aldrich) containing Puromycin (stock solution 25 mg/mL, Sigma-Aldrich) with a final concentration of 25 μg (1μL of stock solution) of puromycin in 5mL of Schneider's insect medium. During dissection, Malpighian tubules and crop were kept attached to the gut and precaution was taken to keep the intestines intact. Guts were then incubated at room temperature in puromycin containing medium for 45 min. After incubation, standard immunochemistry protocols were applied.

Drosophila protein expression time course

Flies were fed with fed on filters soaked in 5% sucrose only *Pe* (OD_{600} = 25). Half of the flies were dissected following 16h post-infection. The second half was flipped on regular food and dissected 24h later (recovery).

Fluorescence-activated single-cell sorting

Control flies and flies expressing RNAi against *aub* were collected between 2 and 3 days after hatching and kept at 18°C for 5 days before being transferred to 29°C. Flies were kept are 29°C for 7 days and were flipped into fresh food vials every two days. Fly guts were dissected in cold PBS 16 h after animals being fed with 5% sucrose only or 5% sucrose containing *Pe*. The crop, the Malpighian tubules and the hindgut were carefully removed. Midguts were then collected and transferred in an Eppendorf containing 400 μL of PBS and kept on ice. Each Eppendorf contained roughly 100 midguts. Once all the tissue was dissected, 10 μL of elastase (Sigma-Aldrich, 10 μg/μL) was added to each Eppendorf. Samples were kept at 27°C in a heat block for at least 1 h until midguts were fully dissociated. Tissues were further disrupted by pipetting up and down every 5 min. Samples were then centrifuged at 300 rcf for 20 min at 4°C. After removing the supernatant, the pellet was resuspended in cold PBS. To eliminate enterocytes as much as possible, the cell suspension was filtered with a 30 μm filter (Sysmex). 500 μL of cold PBS were added to wash the filter. After filtration, samples were ready for sorting. Sorting was performed by the CRUK Scotland Institute flow cytometry facility on a FACSAria Fusion Flow Cytometer (BD Biosciences). GFP or Red stinger positive controls were used to set up the flow cytometer parameters that were used for all the conditions. In parallel to the sorting, a few microliters of samples were taken and stained with 20 μL of DAPI to visualize cell death. Between 250 and 500 flies were dissected per condition, resulting in 250,000 to 750,000 sorted cells. Three biological replicates were dissected for each condition. Sorted cells were pelleted by centrifugation at 300 rcf for 20 min at 4°C. After carefully removing the supernatant, 800 μL of TRIzol (Invitrogen) was added to the samples, followed by RNA extraction and sequencing.

Small RNA-sequencing

Small RNA sequencing was performed on either whole midguts, ovaries or sorted ISCs/EBs. For small RNA preparation from whole midguts, flies were dissected in cold PBS 16 h after being fed with 5% sucrose only or 5% sucrose containing *Pe*. The crop, the Malpighian tubules and the hindgut were carefully removed. Three replicates of 40 midguts each were dissected for each condition. Guts were then collected and transferred to an Eppendorf containing 400 μL of PBS and kept on ice. Once all the tissue was dissected, 10 μL of elastase (Sigma-Aldrich, 10 μg/μL) was added to each Eppendorf. Samples were kept at 27°C in a heat block for at least 1 h until the guts were totally degraded. Tissues were disrupted by pipetting up and down every 5 min. Samples were then centrifuged at 300 rcf for 20 min at 4°C. After removing the supernatant, the pellet was resuspended in 800 μL of TRIzol (Invitrogen). The same

protocol was applied for the ovaries. Approximately 10 pairs of ovaries were dissected. We generated small RNA libraries from 1–5 μg of total RNA using a modified protocol from the original method.[125] 19 to 35 nucleotides-long RNA was first selected by PAGE using radiolabeled 19mer spike (5′-CGUACGCGGGUUUAAACGA) and 35mer spike (5′-CUCAUCUUGGUCGUACGCGGAAUA GUUUAAACUGU). The size-selected RNA was precipitated, oxidised by sodium periodate,[126] and size-selected for the second time by PAGE. The size-selected oxidised small RNAs were ligated to the 3′ adapter from IDT (5rApp/NNNNAGATCGGAAGAGCA CACGTCT/3ddC where Ns are randomised) using the truncated T4 RNA Ligase 2, truncated KQ (NEB), followed by a third PAGE to remove non-ligated adapters. Subsequently, the RNA was ligated to the 5' adapter from IDT (ACACUCUUUCCCUACACGACGCUC UUCCGAUCUNNNN where Ns are randomised) using the T4 RNA Ligase 1 (NEB). Adapter-ligated RNA was reverse-transcribed by SuperScript II (Thermo Fisher) and amplified by KAPA LongRange DNA polymerase (Sigma, KK3502) using the universal forward primer, Solexa_PCR-fw: (5′-AATGATACGGCGACCACCGAGATCTACACTCTTTCCCTACACGACGCTCTTCCGATCT) and the barcode-containing reverse primer TruSeq_IDX: (5′-CAAGCAGAAGACGGCATACGAGATxxxxxxGTGACTGGAGTTCAGACGTGTGCT CTTCCGATCT where xxxxxx is the reverse-complemented barcode sequence). Amplified libraries were multiplexed and sequenced on a HiSeq platform in the paired-end 150 bp mode by GENEWIZ/Azenta.

Small RNA-sequencing analysis

The R1 sequencing reads were trimmed of the Illumina-adapter sequence using the FASTX-Toolkit from the Hannon Lab (CRUK Cambridge Institute). The 4 random nucleotides at either ends of the read were further removed. The trimmed reads of 18–40 nt in size were first mapped to the infrastructural RNAs, including ribosomal RNAs, small nucleolar RNAs (snRNAs), small nuclear RNAs (snoRNAs), microRNAs, and transfer RNAs (tRNAs) using Bowtie 1.2.3 allowing up to one mismatch. Sequences annotated in the dm6 r6.31 assembly of the *Drosophila melanogaster* genome were used. The trimmed and unfiltered reads were then mapped to the dm6 genome using Bowtie allowing up to one mismatch. Reads that uniquely mapped to the genome were analyzed for the tile analysis. Reads that mapped to the 100 nt upstream and downstream genomic regions of tRNA, snRNA and snoRNA insertions as well as those that mapped to the *aubergine* gene locus were removed from the tile analysis. Bedtools 2.28.0 was used to count the coverage of the mapped reads. Endogenous siRNA reads (annotated as hpRNA) were used for normalisation. The trimmed and unfiltered reads were separately mapped to the curated sequences of *Drosophila melanogaster* transposons,[57] using Bowtie allowing up to three mismatches with the option of –all –best –strata. The size distribution of the transposon-mapping reads was made using ggplot2 3.4.4 in R 4.0.0. Nucleotide frequencies around the first nucleotide position of antisense and the tenth nucleotide position of the sense transposon-mapping piRNA reads (longer than 22 nucleotides) were counted and visualised using weblogo 3.7.8. Frequencies were measured in the window of 11 nucleotides, and the z scores were calculated as the deviation of the frequency value at the first (antisense reads) and tenth (sense reads) positions from the mean frequency divided by the standard deviation of the frequencies. Small RNA sequencing libraries from Siudeja et al.[56] were analyzed in the same way except for using the adapter sequence TGGAATTCTCGGGTGCCAAG and not trimming the 4 nucleotides at either end.

PolyA-selected RNA-sequencing

Polyadenylated RNA was purified from the DNase-treated total RNA using the oligo d(T)25 magnetic beads (NEB, S1419) and used for the library preparation. Libraries were cloned using the NEBNext Ultra Directional II RNA Library Prep Kit for Illumina (NEB, E7760), following the manufacturer's instruction, and amplified by KAPA polymerase using the same primers as for the small RNA sequencing.

PolyA-selected RNA analysis

Both R1 and R2 reads from the polyA-selected RNA sequencing reads were trimmed of the Illumina-adapter sequences using the FASTX-Toolkit. The trimmed reads were subsequently filtered by the sequencing quality. Only the paired and unfiltered reads were then mapped to the dm6 r6.31 transcriptome combined with curated sequences of *Drosophila melanogaster* transposons using salmon/1.1.0 with the options of –validateMappings –incompatPrior 0.0 –seqBias –gcBias. Length-normalised transposon mRNA reads per one million transcripts including host mRNAs were compared between different libraries. polyA-selected RNA sequencing libraries from ovarian samples from Senti et al.[57] were also analyzed in the same way.

RNA extraction and RT-qPCR

Drosophila tissues

Total RNA was extracted from tissues dissected in cold PBS. Three or four replicates of 20–40 guts were dissected for each condition. Depending on the experiments, sorted ISCs/EBs cells, R4-R5 regions, ovaries and/or whole guts were homogenised in 100 μL of Trizol (Thermo Fischer Scientific) using a mortar and a pestle first, followed by adding further 700 μL of Trizol. 200 μL of Chloroform was added and mixed well with Trizol by vortexing before centrifugation on a bench top centrifuge. The aqueous phase was saved, and RNA was precipitated with iso-propanol. RNA was treated with DNase (Thermo Fischer Scientific) and quantified using a NanoDrop Spectrophotometer. About 1 μg of RNA was converted to cDNA using a high-capacity cDNA reverse transcription kit (Thermo Fisher Scientific). RT-qPCR was performed using Perfecta SYBR green fast mix (Quantabio) as per the manufacturer's instructions on an Applied Biosystems QuantStudio 3 fast real-time PCR system and each reaction was carried out in triplicates. A standard curve was created using 1:10 dilutions from pooled cDNA samples. The amount of sample was extrapolated from this

standard curve and normalised using data from the housekeeping gene *rpl32*. Melting curves were conducted priorly to ensure only one product was formed from each pair of primers. Data was exported and analyzed in excel. The results are shown as the ratio of average of mRNA levels of the candidate gene/*rpl32*.

Intestinal organoids

RNA samples from 3 biological replicates were isolated by using RNeasy Mini Kit (Qiagen #74106) following manufacturer's protocol. RNA samples were subsequently treated with RNase-Free DNase Set (Qiagen, #79254). RNA samples were analyzed for quality and quantity using Thermo Scientific Nanodrop (Thermo Fisher). 500ng RNA used for cDNA generation using qScript cDNA SuperMix (VWR, #95048–100). The results are shown as the ratio of average mRNA levels of the candidate gene/*β-actin*.

TCGA analysis

To study *PIWIL1* RNA expression across the different CMS subtypes of CRC or according to the microsatellite status of the patients, we took advantage of the TCGA datasets from the PanCancer Atlas. Analysis has been performed on open access data from colonic adenocarcinoma patients only. Differential gene expression was then assessed, and statistics have been performed using Graphpad.

Samples visualization and image acquisition

PH3 counting was performed using a BX51 Olympus. Fluorescence images of *Drosophila* intestines were acquired using a confocal Zeiss 710 or a Zeiss LSM 780. Stained TMAs slides were scanned and analyzed using the HALO system (indica labs).

QUANTIFICATION AND STATISTICAL ANALYSIS

Immunofluorescence staining

Quantification of ISC proliferation was done by manually counting the number of PH3-positive cells per posterior midguts. Quantification of Arm, eIF3C, eIF4G, Multiubiquitination, Myc, Puromycin, Sox21a and Wg staining was performed by measuring the mean fluorescence intensity of the protein in all GFP positive cells on a SUM or MAX projection generated via Fiji. Prior the measurement, a mask was created via Fiji to delineate the GFP positive cells only, using the tool "Create a selection". In parallel, mean fluorescence intensity of the background was measured on a specific region of interest on each SUM projection and subtracted from the signal measured in the cells.

Quantification of Aub staining was performed by measuring the mean fluorescence intensity per cell on a SUM projection done by Fiji. This measure was blindly performed in three different GFP positive cells per gut for Aub. In parallel, mean fluorescence intensity of the background was measured on a specific region of interest on each SUM projection and subtracted from the signal measured in the cell. This quantification was repeated in 5 different guts per biological replicate.

In the rescue experiments (aub^{WT}, aub^{AA} and aub^{ADH}), GFP and Aub staining were quantified by measuring the mean fluorescence intensity of the protein in all GFP positive cells on a MAX projection realised via Fiji. Prior the measurement, a mask was created on Fiji to delineate the GFP positive cells only via using the tool "Create a selection". In parallel, mean fluorescence intensity of the background was measured on a specific region of interest on each SUM projection and subtracted from the signal measured in the cells. Quantification of the % of GFP positive area was measured using the same mask and divided by the gut area, measured with the DAPI staining.

MARCM clones

Quantification of ISC proliferation in MARCM clones was performed by manually counting the number of DAPI positive cells in each GFP-positive clone. The statistics were done with GraphPad Prism 6. The tests used for each experiment are described in the figure legends.

Transcriptional profiling of patient tissue

The Glasgow cohort consisted of $n = 787$ stage 1–3 CRC patients who underwent surgery with curative intent within Greater Glasgow and Clyde between 1997 and 2013. Formalin fixed paraffin embedded tumor resections were annotated for epithelial rich regions. These areas were extracted and profiled for full transcriptome expression using TemOSeq as previously described.[127] Patients were excluded from analysis due to mortality within 30 days of surgery. Raw gene counts were normalised using DESeq2 in RStudio. *PIWIL1* expression was assessed for association with TNM stage via Kruskal Wallis testing in GraphPad prism version 10. Data were dichotomised into high and low expression groups using the *Survminer* package in R Studio. Kaplan Meier survival analysis was performed using the *Survival* package in R Studio. This study was approved by the Research Ethics Committee of the West Glasgow University Hospitals NHS Trust (NHS GG&C REC ref. 22/WS/0020), in accordance with Human Tissue (Scotland) Act 2006, which included policy on consent. Data were deposited and accessible within Glasgow Safehaven (GSH21ON009).

Statistics

Detailed statistical information for each experiment within the study is provided within the figure legends. In all cases data represent the mean ± SD. ns, not significant ($p > 0.05$); *$p < 0.05$, **$p < 0.01$, ***$p < 0.001$ and ****$p < 0.0001$.